SOLARISE project

Accelerating solar energy adoption

Interreg
EUROPEAN UNION
2 Seas Mers Zeeën
European Regional Development Fund

CO2
Low-carbon technologies

TOTAL PROJECT BUDGET:
4.35 M €
INCLUDING AN ERDF BUDGET OF:
2.61 M €

Modeling & Control of a PVT

Ahmed Rachid

Professor

Université de Picardie Jules Verne

www.interregsolarise.eu

Content

2

Introduction

What is a PV-T ?

- Combines PV and ST modules into one integrated panel
- Provides heat and electricity simultaneously
- Solar cells and a thermal module
- Role of heat transfer medium in heat extraction.

Why PV-T ?

- Energy demand
- Global warming
- Heat and electricity simultaneously
- Total efficiency of more than 50%.

Advantages

- Less bulky
- Simple operation
- Mediums found abundantly
- Work in all temperature.

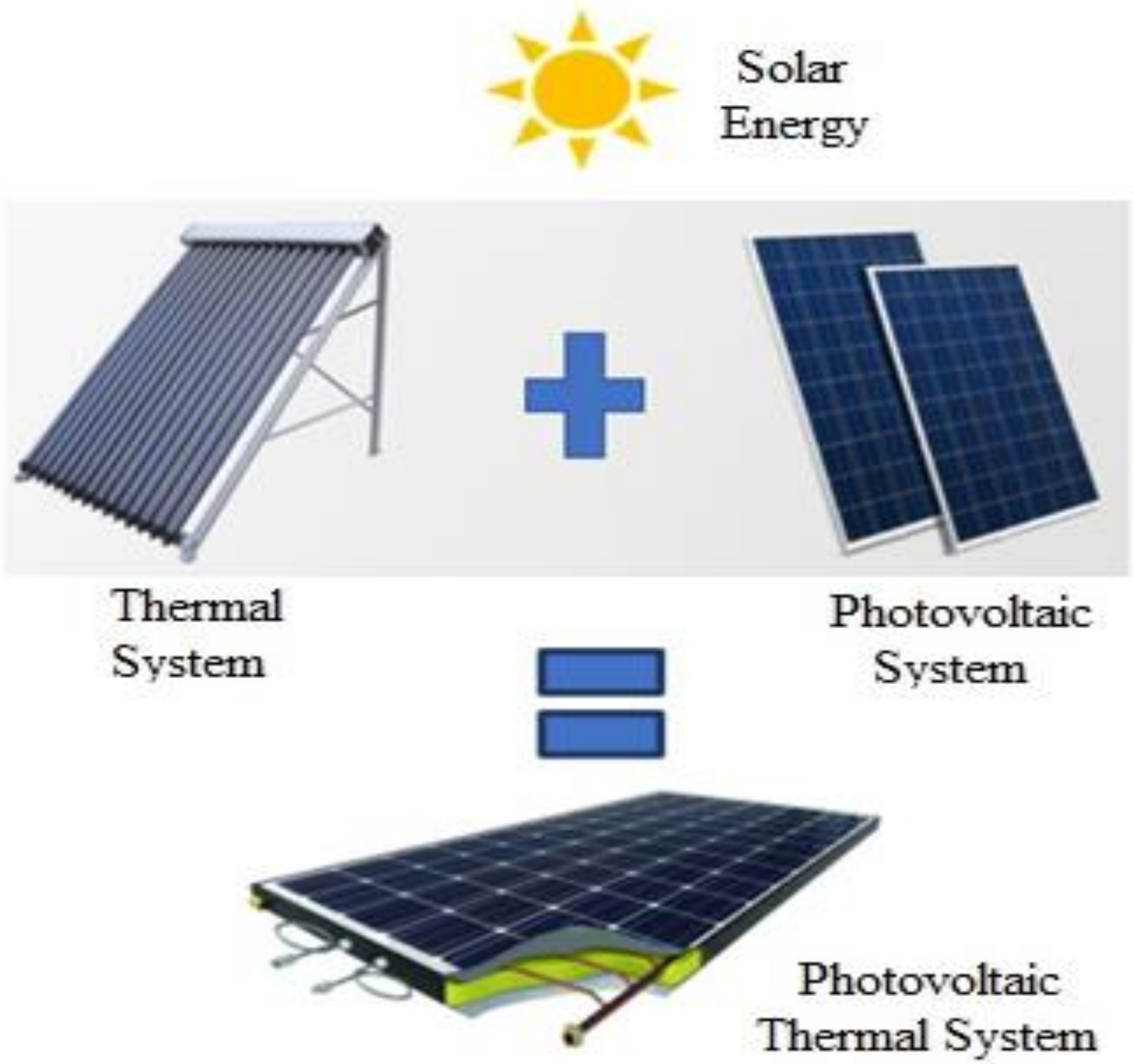

Basic working principle of PV-T collector.

Introduction

- Mainly composed of solar cells, heat exchanger and fluid + Other optional components can be added.

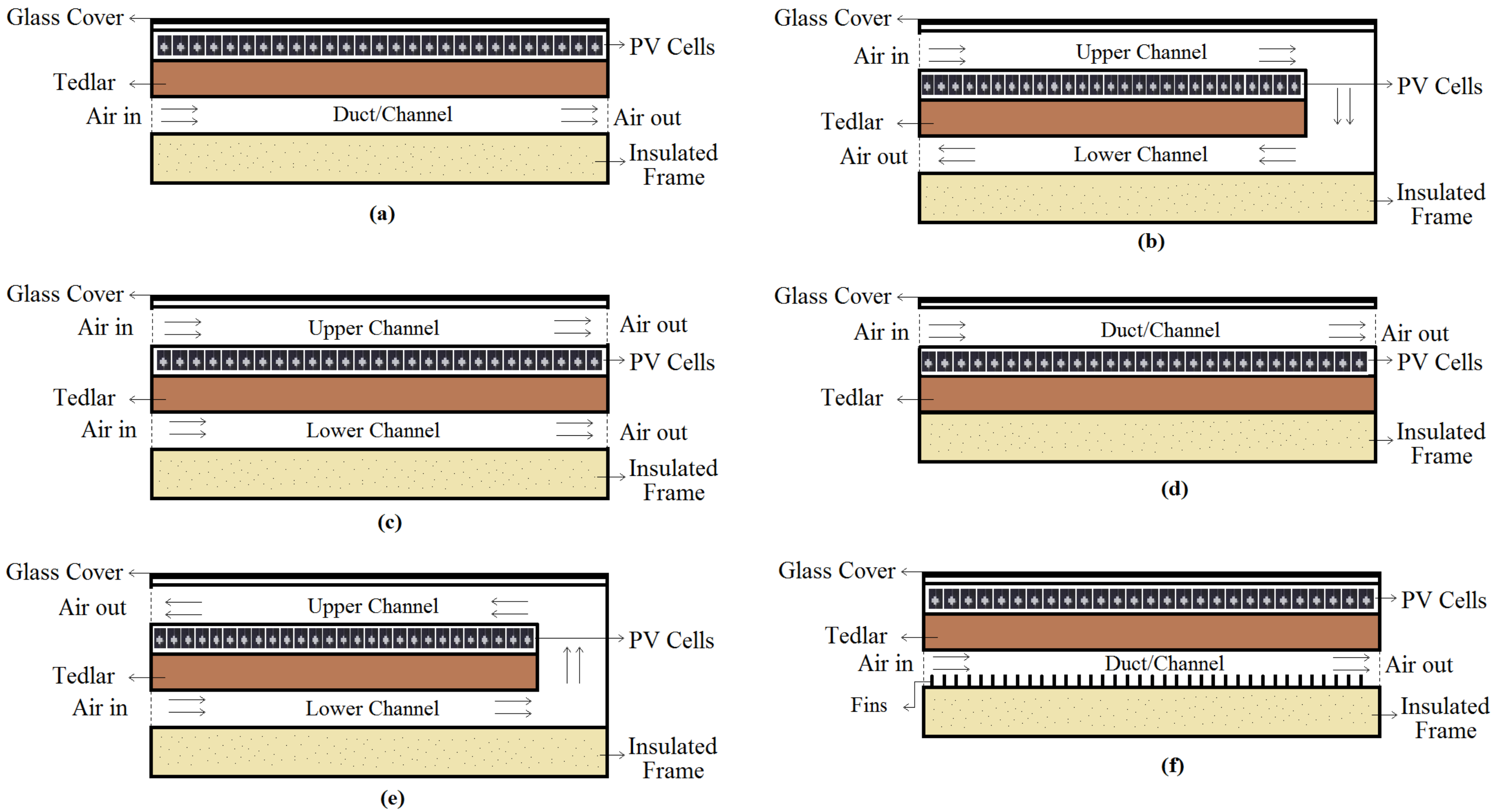

Different configurations of air-based PV-T collectors.

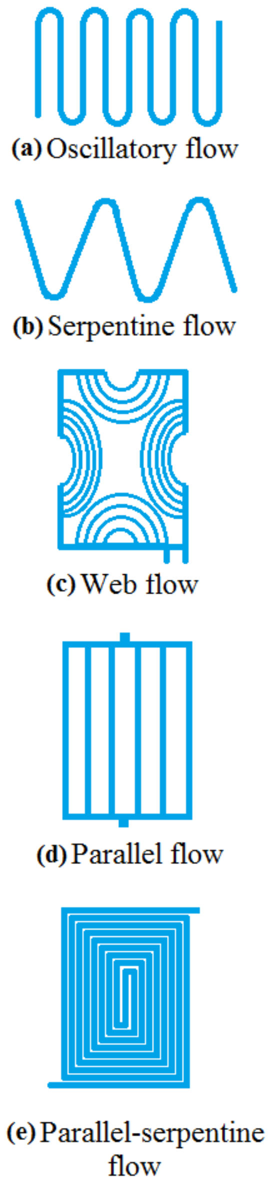

Flow passages in a liquid-based PV-T collector.

Modeling

- Different configurations of hybrid PV-T collectors are considered
- Requires a thorough study of heat transfer
- Focus is to present a dynamic model
- Few assumptions are made
- Approach is based on a bond graph technique
  - *represented by symbols and lines*
  - *resistance, compliance, and inertance*
  - *multiple domains*
  - *sources*
  - *effort and flow*
  - *junctions.*

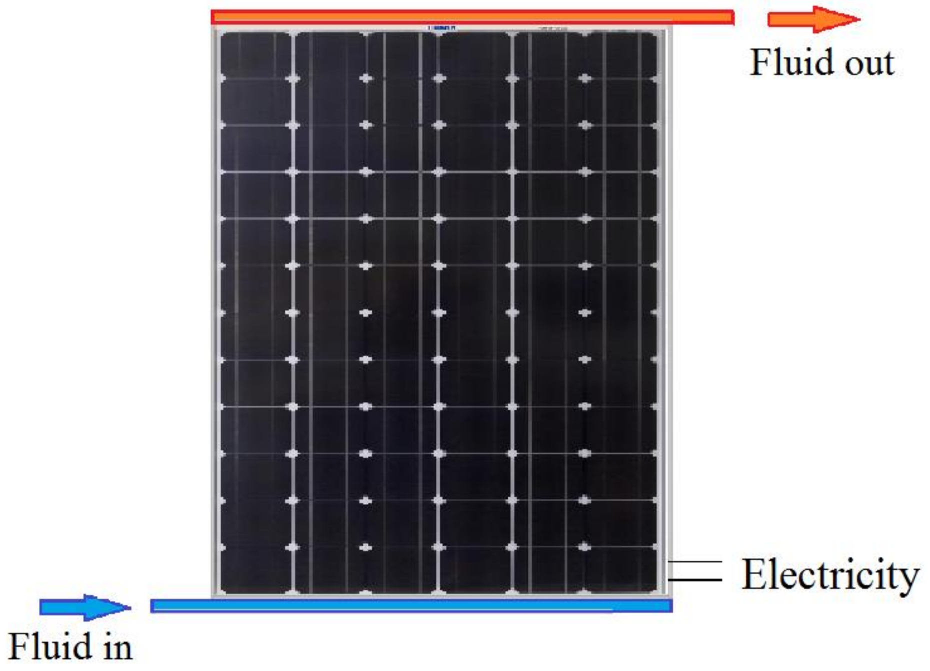

Overall view of a PV-T collector.

	0-junction	1-junction
flow equation	$\sum_{k=1}^{m} f_{ik} = \sum_{k=1}^{n} f_{ok}$	$f_{i1} = \ldots = f_{im} = f_{o1} = \ldots = f_{on}$
effort equation	$e_{i1} = \ldots = e_{im} = e_{o1} = \ldots = e_{on}$	$\sum_{k=1}^{m} e_{ik} = \sum_{k=1}^{n} e_{ok}$

Flow and effort expressions for junctions.

Modeling

- Dynamic thermal model of a water-based PV-T collector

$$M_g C_g \frac{dT_g}{dt} = A_{mod}[\alpha_g I_{sun} - h_{r,gs}(T_g - T_s) - h_{v,am}(T_g - T_{am}) - h_{c,gc}(T_g - T_c)]$$

$$M_c C_c \frac{dT_c}{dt} = A_{mod}[\tau_g \alpha_c I_{sun} \beta + h_{c,gc}(T_g - T_c) - h_{c,ct} \ (T_c - T_t)] - E_p$$

$$M_t C_t \frac{dT_t}{dt} = A_{mod} h_{c,ct}(T_c - T_t) - A_{tm} h_{c,tm}(T_t - T_m) \ - A_{tr} h_{c,tr}(T_t - T_r)$$

$$M_r C_r \frac{dT_r}{dt} = A_{tr} h_{c,tr}(T_t - T_r) - A_{rm} h_{c,rm}(T_r - T_m) - A_{ri} h_{c,ri}(T_r - T_i)$$

$$M_m C_m \frac{dT_m}{dt} = A_{tm} h_{c,tm}(T_t - T_m) + A_{rm} h_{c,rm}(T_r - T - A_{mi} h_{c,mi}(T_m - T_i) - A_{mw} h_{v,mw}(T_m - T_w)$$

$$M_w C_w \frac{dT_w}{dt} = A_{mw} h_{v,mw}(T_m - T_w) + \dot{m}_w C_w (T_{wi} - T_{wo})$$

$$M_i C_i \frac{dT_i}{dt} = A_{mi} h_{c,mi}(T_m - T_i) + A_{ri} h_{c,ri}(T_r - T_i) - A_{mod} h_{v,iam}(T_i - T_{am})$$

- *electric power*

$$E_p = I_{sun} A_{mod} \eta_{ref} \left[1 - \beta_p (T_c - T_{c,ref}) + \delta ln \left(\frac{I_{sun}}{I_{sun,ref}}\right)\right]$$

- *fluid temperature*

$$h^{rd}_{gla/sky} = \sigma \varepsilon_{gla} \frac{T^4_{gla} - T^4_{sky}}{T_{gla} - T_{amb}}$$

$$T_w = \frac{(T_{wi} + T_{wo})}{2}$$

$$h^{rd}_{gla/sky} = \sigma \varepsilon_{gla} \frac{T^4_{gla} - T^4_{sky}}{T_{gla} - T_{amb}}$$

- Thermal model expressed as

$$\begin{cases} \dot{x}(t) = Ax(t) + B(x(t))u(t) + Gv(t) \\ y(t) = Cx(t) + Dv(t) \end{cases}$$

- *state vector*

$$x = [\ T_g \ \ T_c \ \ T_t \ \ T_r \ \ T_m \ \ T_w \ \ T_i\ ]^T$$

- *disturbance vector*

$$v = [\ T_{am} \ \ I_{sun} \ \ T_{wi}\ ]^T$$

- *mass flow is the control input.*

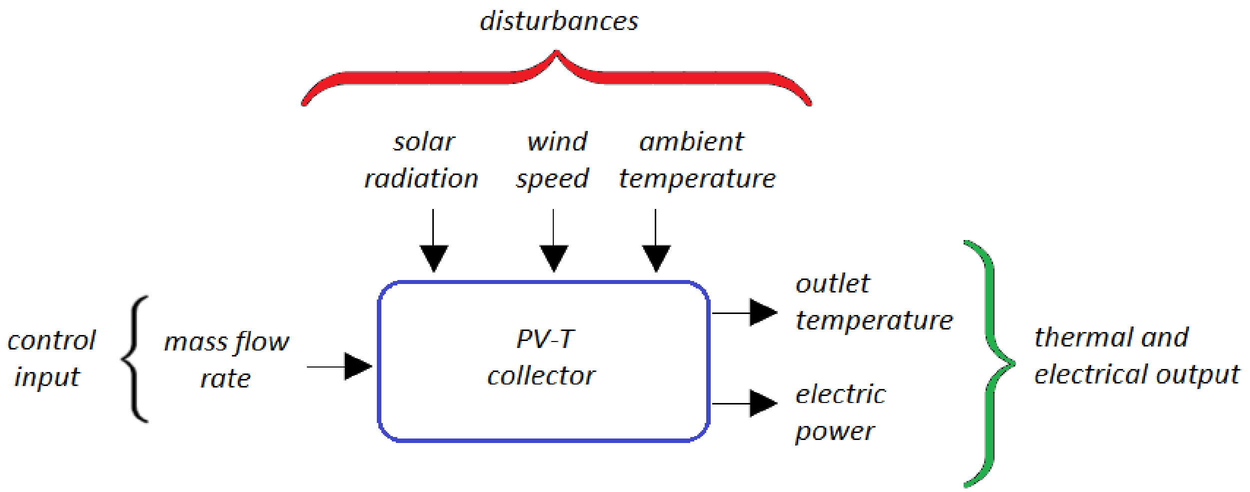

Inputs and outputs of the collector.

Modeling

Air-based model-I

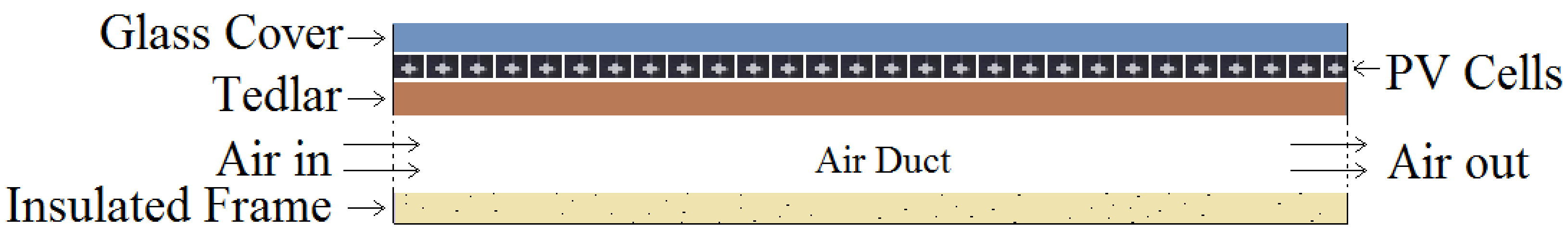

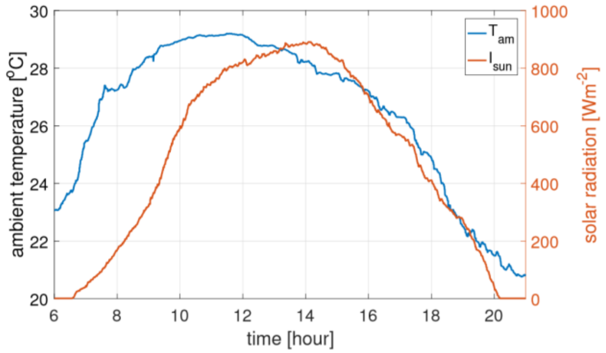

Hourly variation of solar radiation and ambient temperature.

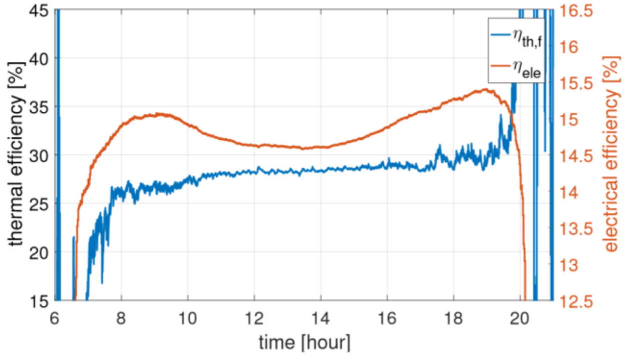

Daily hourly variation of electrical and thermal efficiencies without glazing.

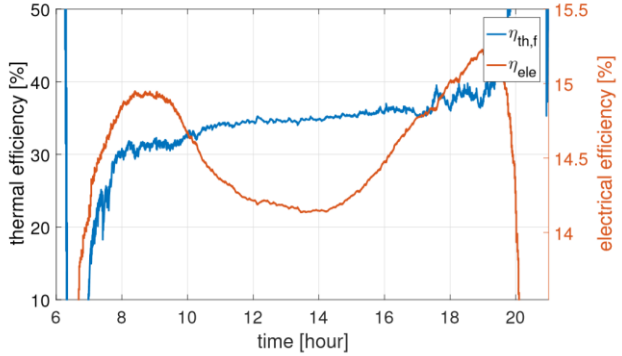

Daily hourly variation of electrical and thermal efficiencies with glazing.

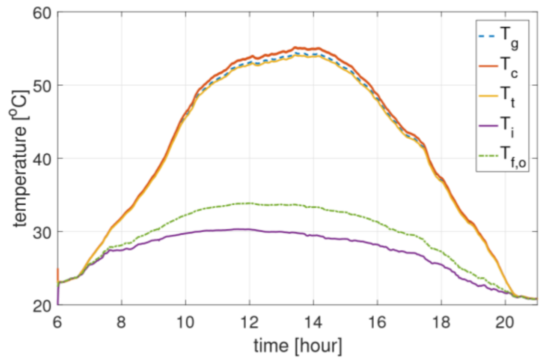

Temperature evolution of PV-T components without an absorber component.

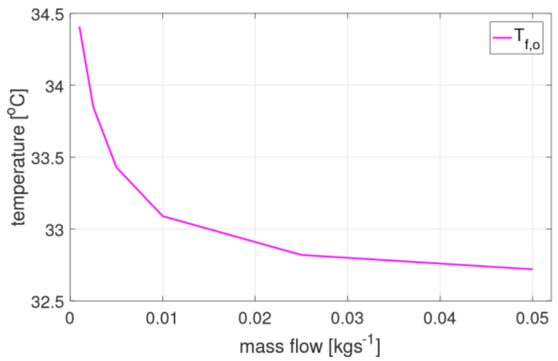

Variation of outlet air temperature with the increase in mass flow rate.

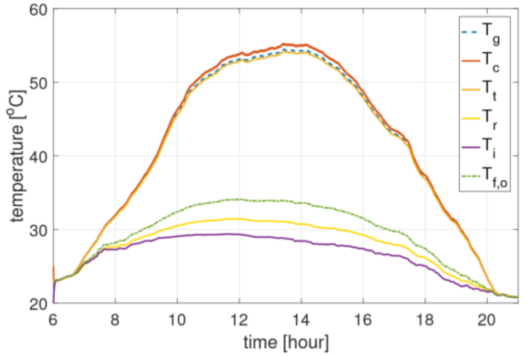

Temperature evolution of PV-T components with an absorber component.

Modeling

Air-based model-II

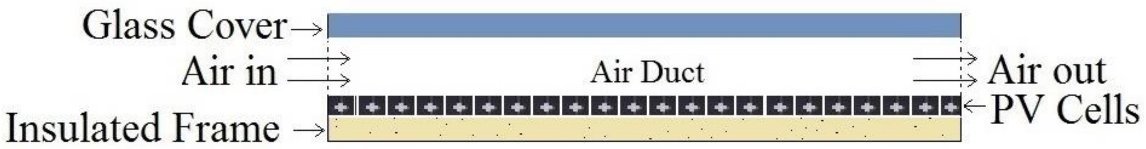

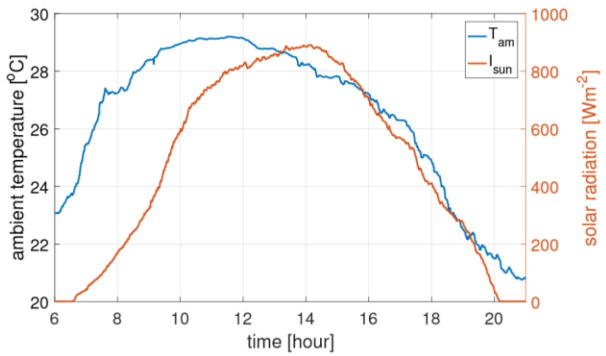

Hourly variation of solar radiation and ambient temperature.

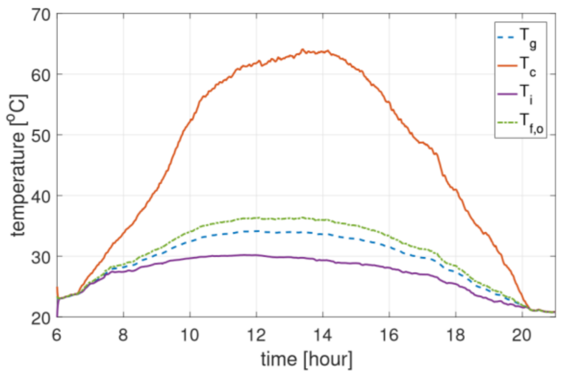

Temperature evolution of PV-T components.

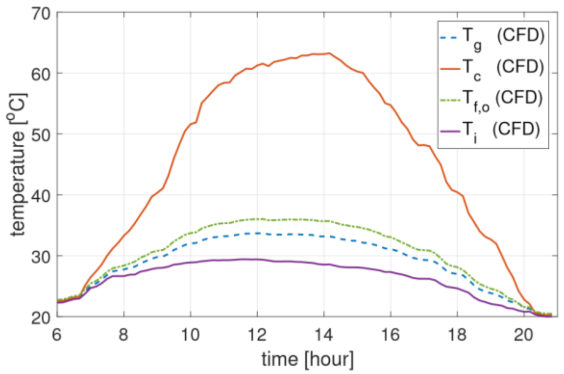

Temperature evolution of a PV-T components (CFD study).

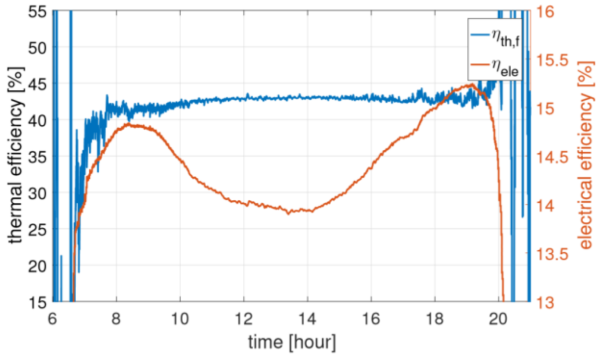

Daily hourly variation of electrical and thermal efficiencies.

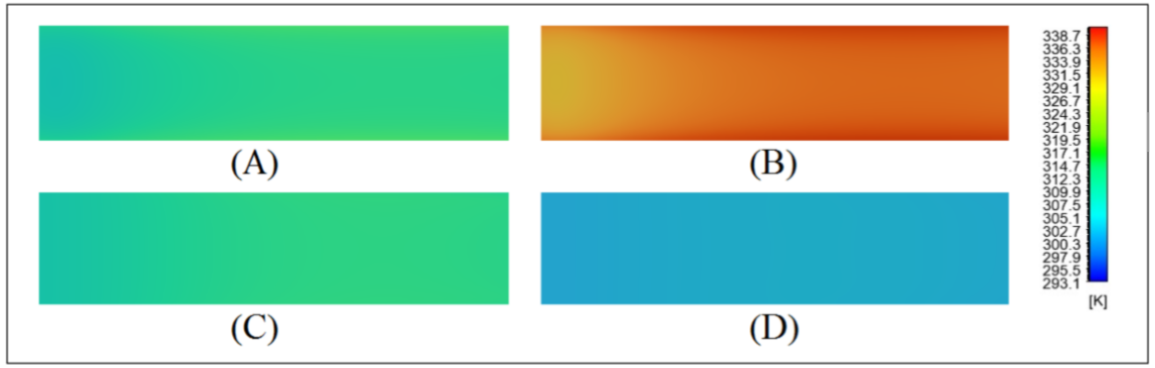

Temperature distributions of the air-based PV-T collector components; (a) Glass cover. (b) PV cell layer. (c) Fluid (air channel). (d) Insulator.

Modeling

Water-based model

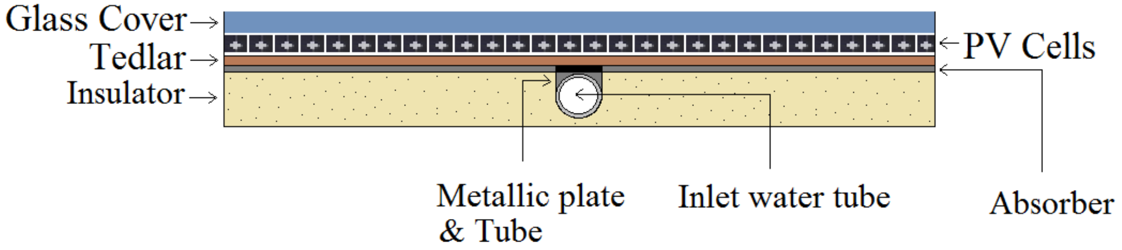

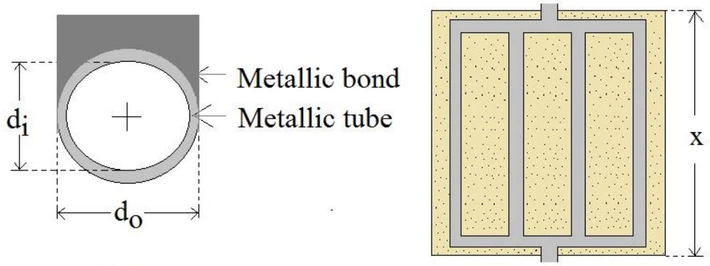

(a) (b)

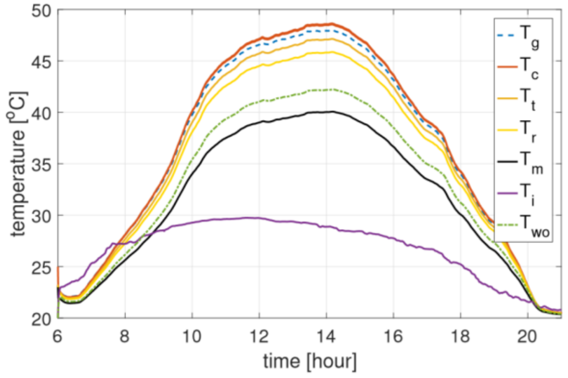

Temperature evolution of PV-T components.

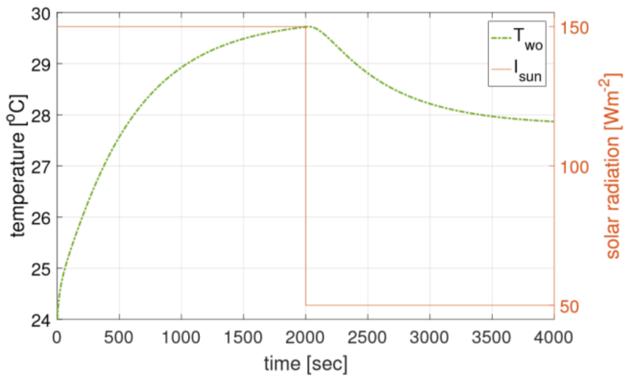

Fluid temperature with a step change in solar radiation.

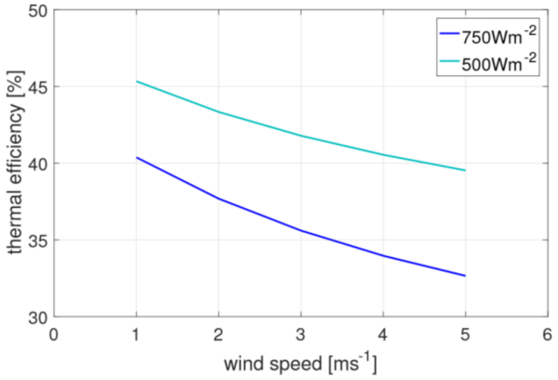

Influence of wind speed on thermal efficiency.

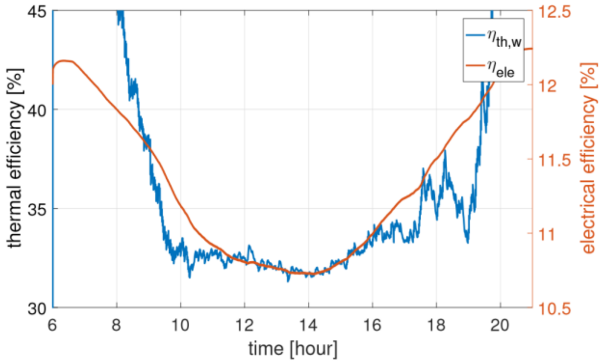

Daily hourly variation of electrical and thermal efficiencies.

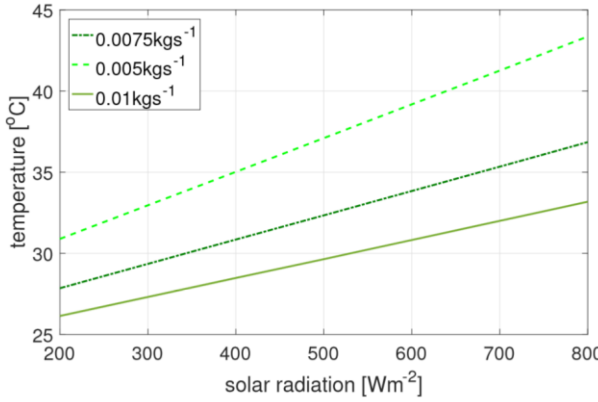

Influence of mass flow rate on the output temperature.

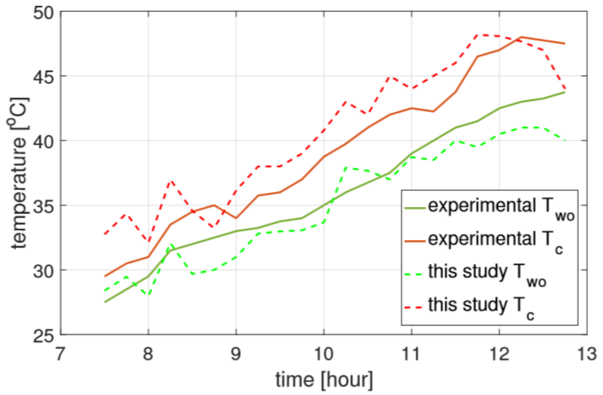

Hourly evolution of temperatures (cell and outlet fluid) both experimentally and theoretically.

Modeling

Decision tree algorithm

- Makes use of input-output data sets to train models
- Regression model is used
- Multi-output decision tree algorithm is implemented.

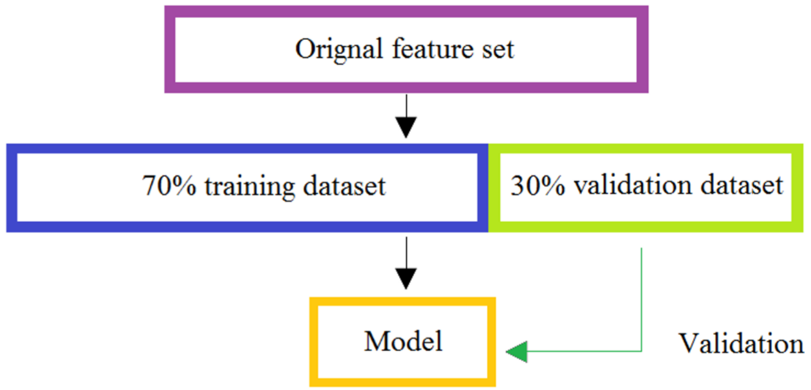

Fig. 41. Schematic representation.

Artificial Neural Network

- High learning ability and capability
- Consists of an input-output layers and at least one hidden layer
- Continued until error is zero or difference is within target threshold.

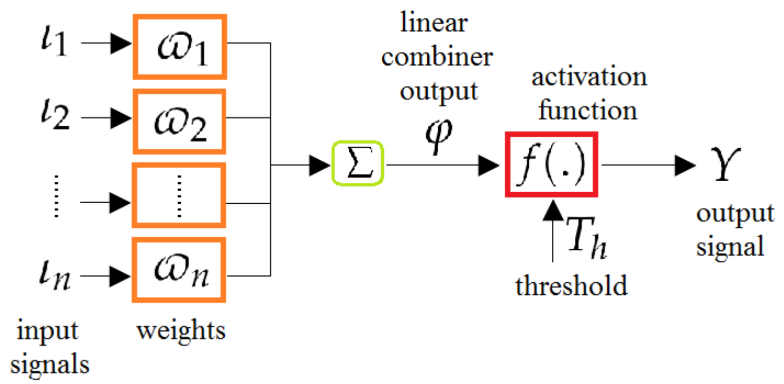

Fig. 42. Basic model of the neural network.

Modeling

Results

- An accuracy score of 75% is achieved for decision tree algorithm

- Root mean square error calculated is 0.107

- Threshold limit or the convergence limit for ANN is $1\text{x}10^{-7}$.

Input variable	I_{sun} (Wm^{-2})	T_{am} (^{o}C)	V_w (ms^{-1})	$\dot{m}_w$ (kgs^{-1})
upper bound	700	31	5	0.05
lower bound	100	21	1	0.005

Lower and upper bounds of input variables.

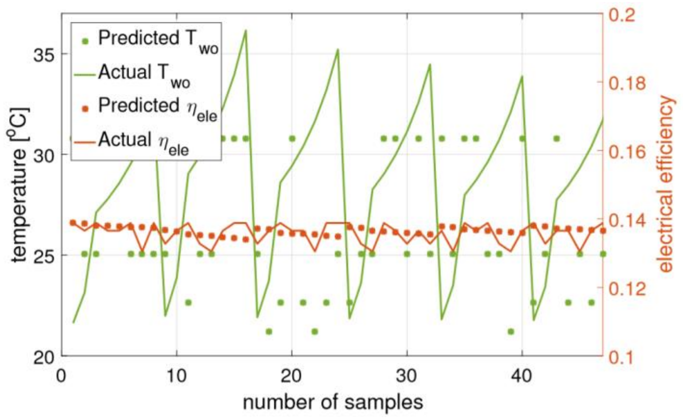

Comparison of actual and predicted outputs using decision tree algorithm.

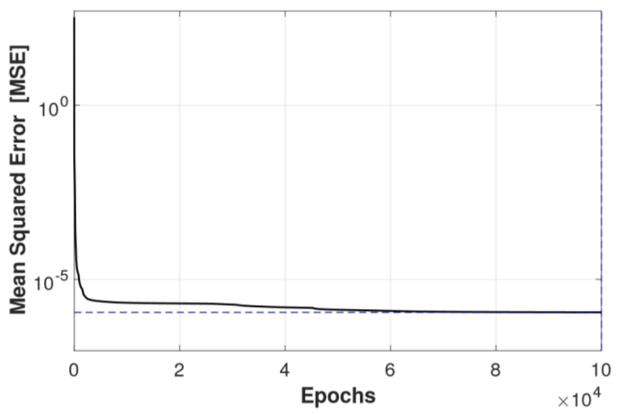

Mean squared error (ANN).

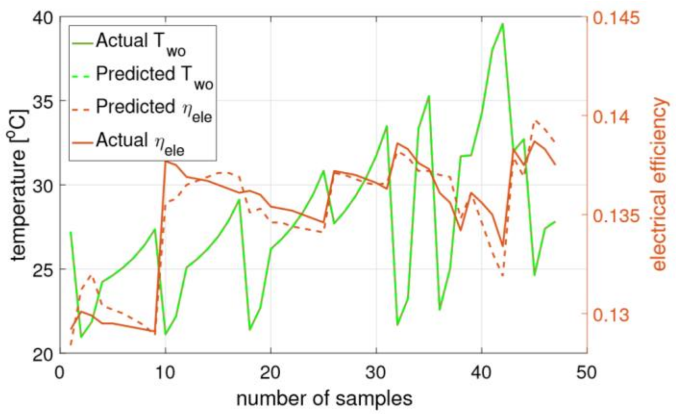

Comparison of actual and predicted outputs using ANN.

Design of innovative PV-T

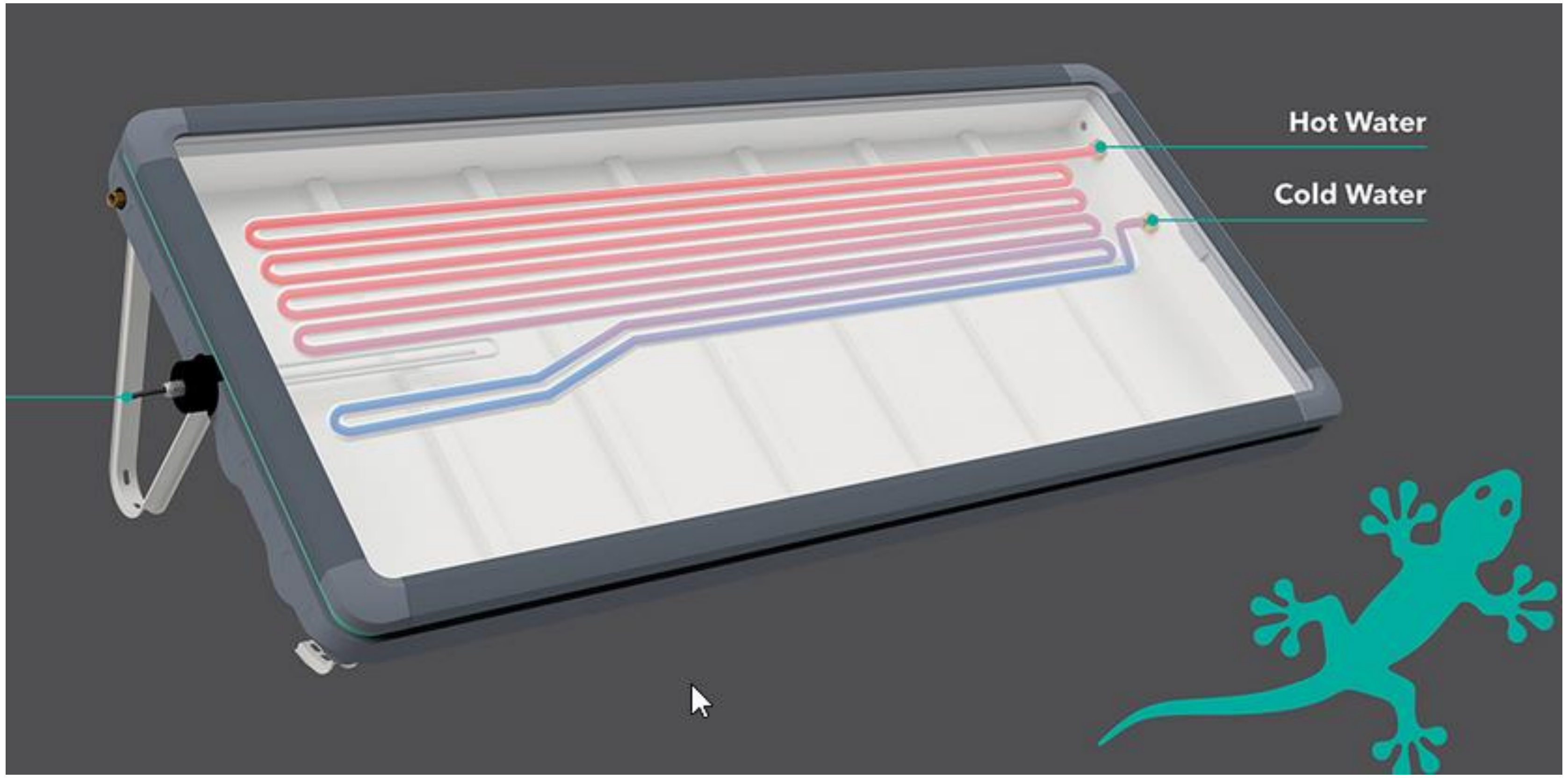

WITH AN ADDITIONAL
1 KW HEAT ROD

Design of innovative PV-T

Geometry of thermal section

- Embedded with storage tank
- Serpentine tube takes the heat from the top
- Heating element is included equipped with electrical resistance wires
- Pump is an additional element and consumes electrical power.

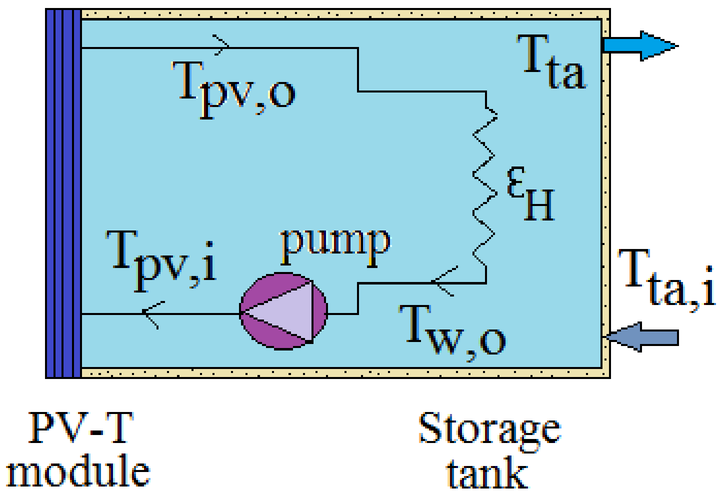

Fig. 46. Schematic diagram of PV-T module integrated with a storage tank.

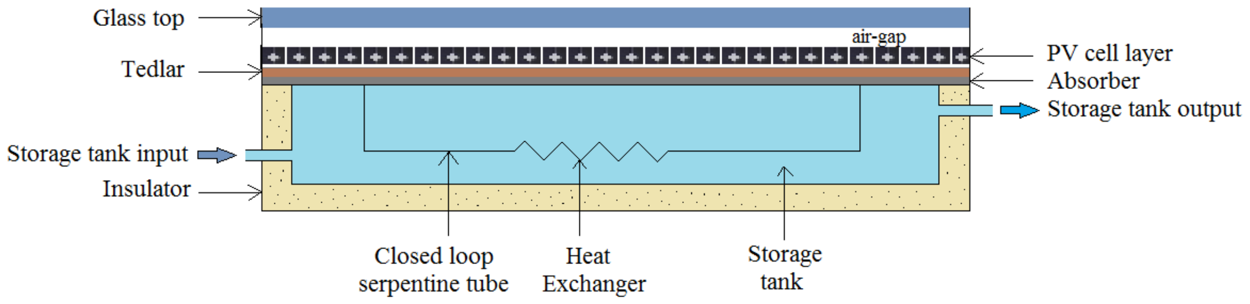

Fig. 47. Cross-section view of PV-T integrated with a storage tank.

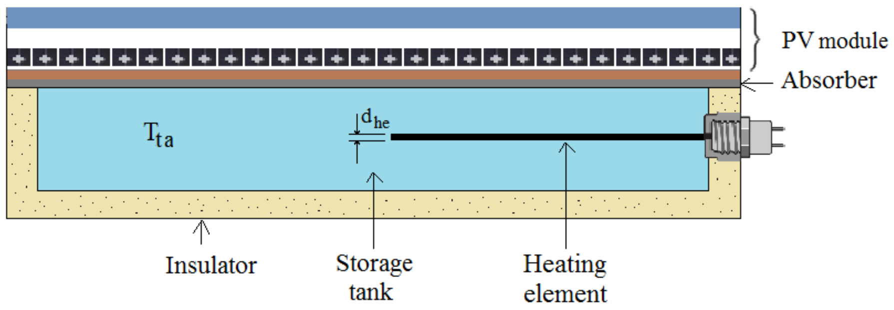

Fig. 48. PV-T system integrated with a heating element.

Design of innovative PV-T

Results - CFD

- CFD model has been setup with boundary conditions
- Assumptions are considered
- Similar temperature distributions can be obtained for other components
- Error found in case-I is 3.40%, 4.10% in case –II and 2.87% in case-III.

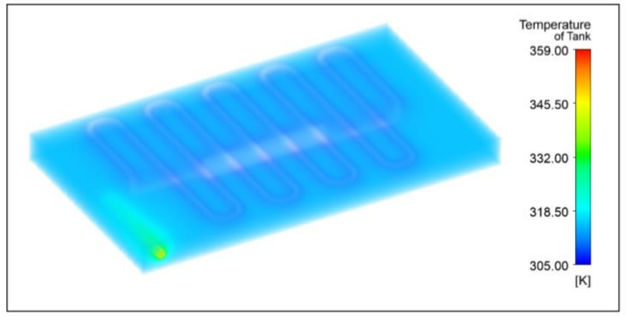

Fig. 54. Temperature distributions of the storage tank fluid incorporating an electric heater.

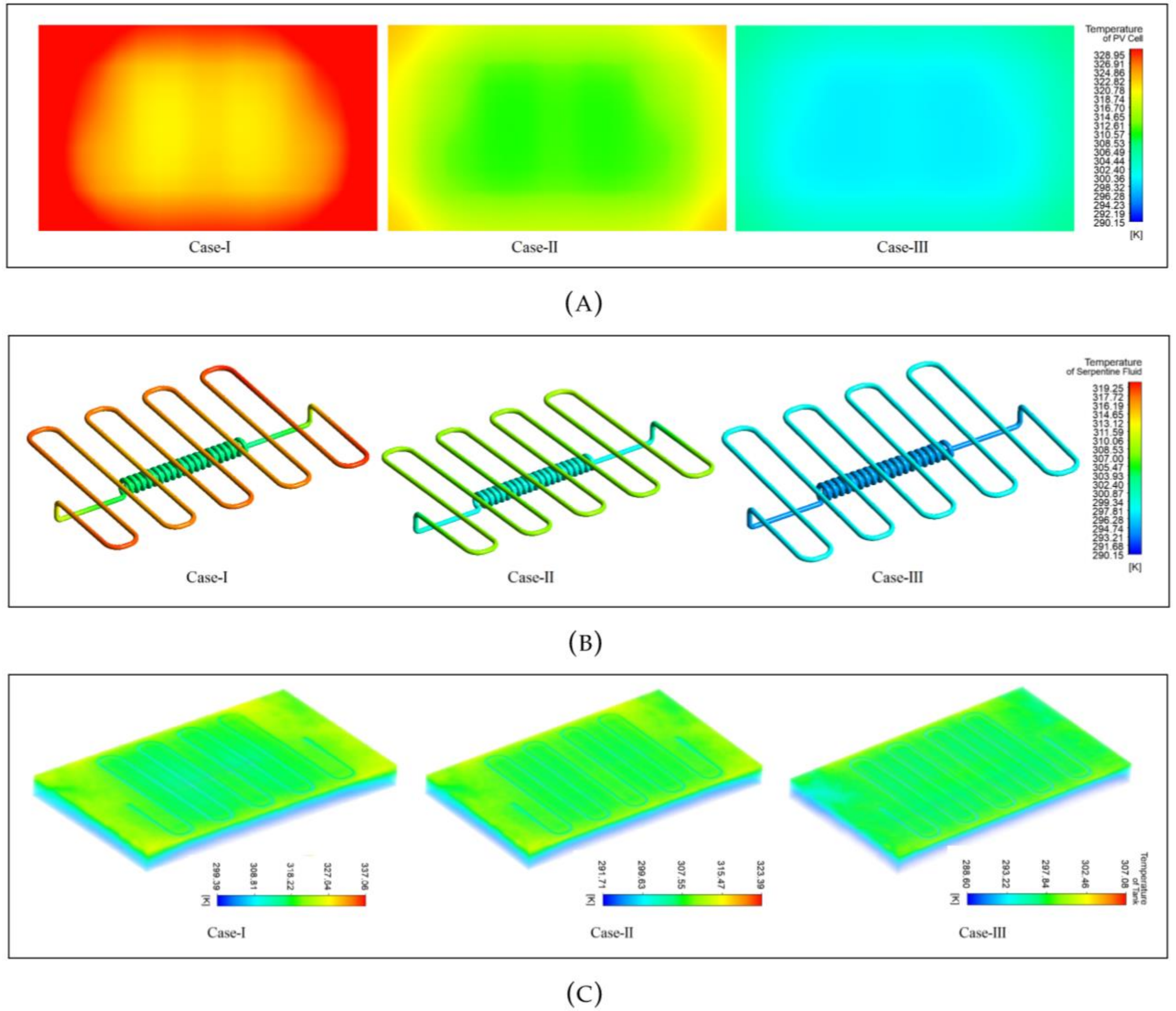

Fig. 55. Temperature distributions (a) PV cell layer. (b) Serpentine tube fluid. (c) Storage tank fluid.

Design of innovative PV-T

Results - Influence

- Material change for absorber and tube
- Thickness of PV-T components
- Fluids for serpentine tube
- Used engine oil as an absorber.

Copper and aluminum.

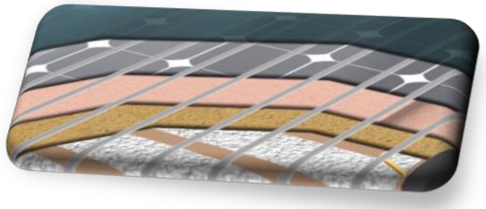

Thickness of absorber and insulator.

Glycol, water and PCM.

Engine oil.

Material	T_w (^oC)
Copper	43.63
Aluminium	43.01

l_{in} (mm)	T_{ta} (^oC)
80	37.10
25	35.63

l_{ab} (mm)	T_w (^oC)
1.00	43.63
0.50	44.39

Fluid	Temperature (^oC)
Pure water	43.63
Pure glycol	46.86
Mixed wt%50	45.45
Paraffin wax	46.63

Component	Temperature (^oC)
Absorber	50.81
S. fluid	41.6

Influence of geometrical parameters.

Optimization

- Genetic algorithm is implemented
- Aim is to maximize the output and reduce the cost for component thickness
- For mass flow, the aim is to maximize output and PV efficiency
- Bounds are set considering real values
- Upper and lower bounds of mass flow are set as 0.05 and 0.005 kgs^{-1}.

Design parameters	l_g (mm)	l_t (mm)	l_r (mm)	$l_i(mm)$
upper bound	5	1.5	2	80
lower bound	2	0.5	0.5	10

Table 5. Lower and upper bounds of the design parameters.

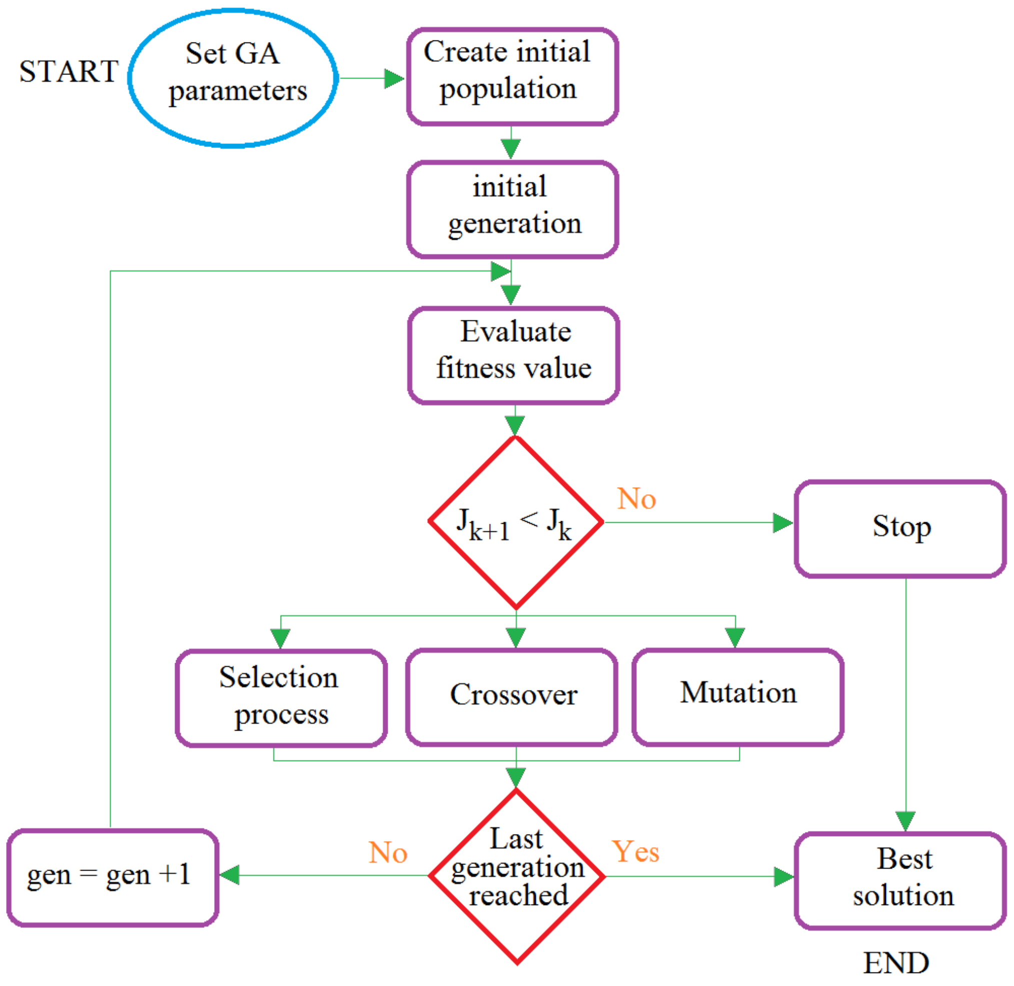

Genetic algorithm flowchart.

Optimization

Results

- Temperatures are calculated considering different thicknesses
- Optimal thickness and mass flow variables are obtained.

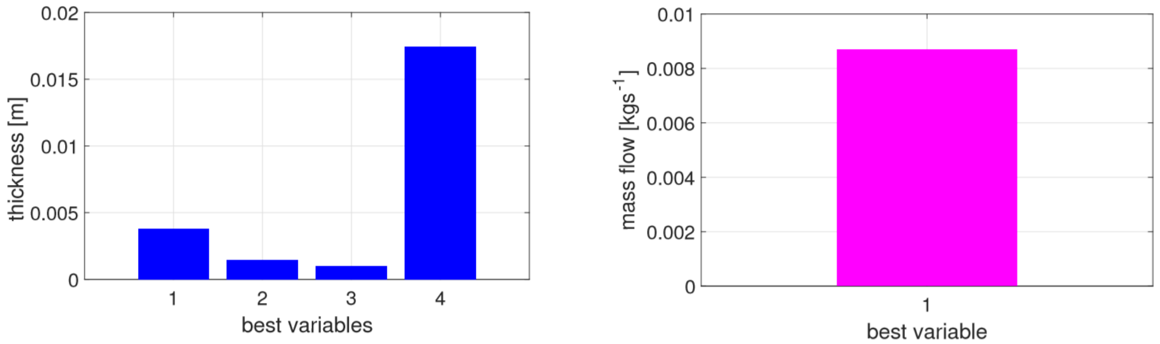

(A) (B)

Fig. 61. (a) Best thickness variables. (b) Best mass flow.

Component	l (m)	T_c (^oC)	T_{wo} (^oC)	η_{ele} (%)
glass (g)	0.002	49.70	43.16	14.97
	0.005	49.92	43.28	14.95
tedlar (t)	0.0005	48.69	44.26	15.04
	0.0015	50.60	42.44	14.90
absorber (r)	0.0005	49.85	43.23	14.95
	0.002	49.70	43.08	14.97
insulator (i)	0.01	48.84	42.21	15.03
	0.08	49.87	43.22	14.95

Table 6. Summary of temperatures and efficiency considering upper and lower bounds.

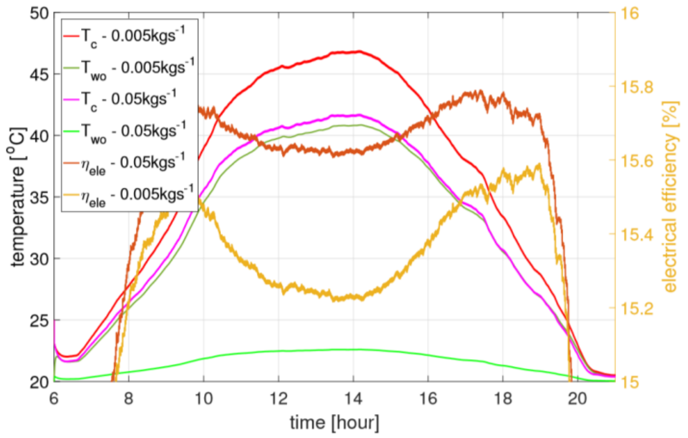

Fig. 62. PV cell, outlet water temperature and PV efficiency evolution with different mass flow.

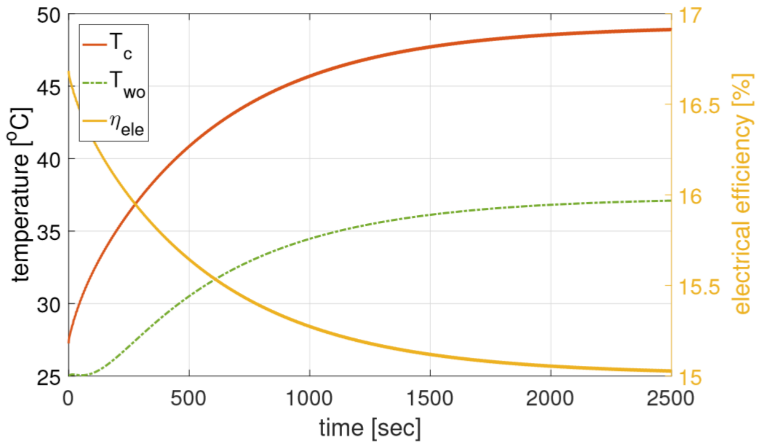

Fig. 63. PV cell, outlet water temperature and PV efficiency with optimized variables.

Control

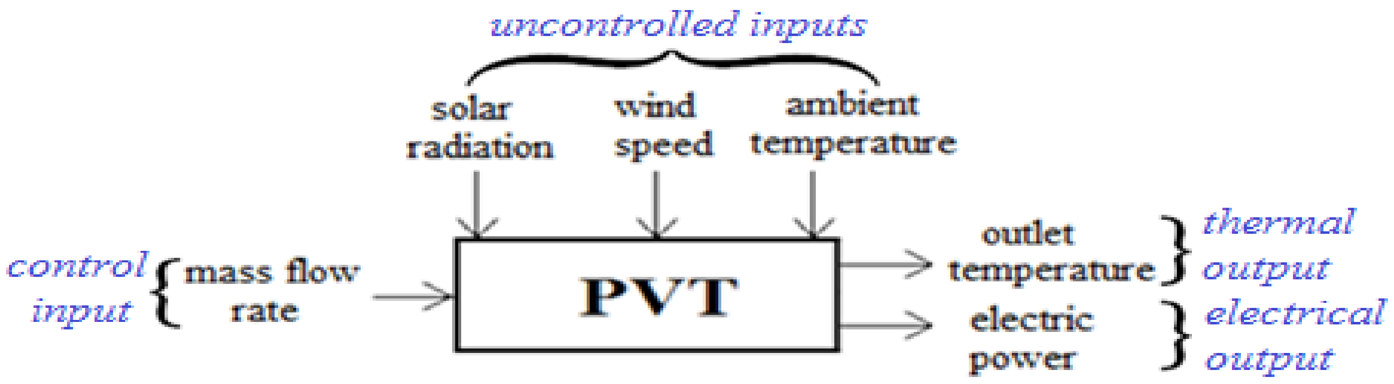

Time constant	{ 31.25, 41.67, 50, 34.48, 47.66 & 76 }
Gain	{ -15, -19.17, -22.5, -14.14, -17.14 & -24.61 }

$$G_{avg}(s) = \frac{T_f}{\dot{m}_f} = \frac{k_{avg}}{1+sT_{avg}} = -\frac{0.42}{s+0.024}$$

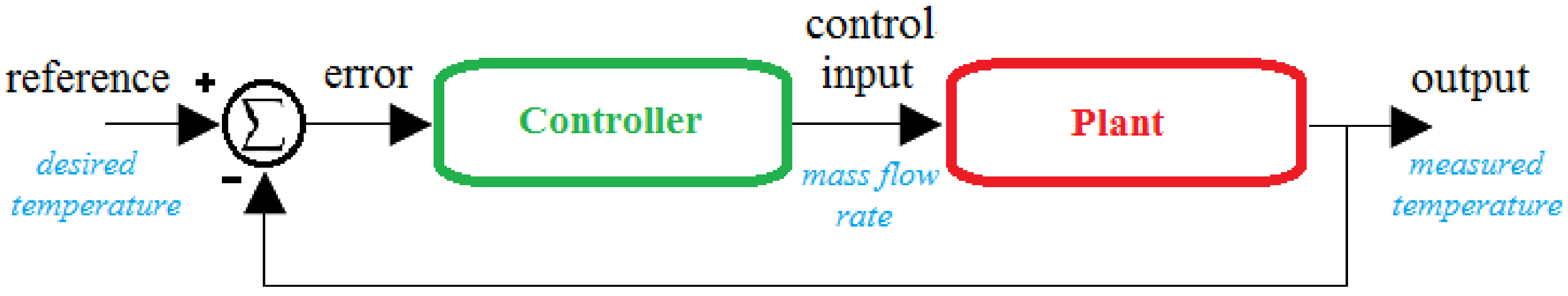

Simple feedback control loop.

Control

- How controller parameters are obtained?

$$G_{avg}(s) = \frac{b}{s+a} \qquad C(s) = K_p + \frac{K_i}{s}$$

- Closed loop transfer function

$$F(s) = \frac{b(K_p s + K_i)}{s^2 + (a + bK_p)s + bK_i}$$

- Controller parameters can be written as:

$$K_p = \frac{2\zeta\omega_o - a}{b} \qquad K_i = \frac{\omega_o^2}{b}$$

- Controller tracks the reference point

- Controller compensates the solar radiation change.

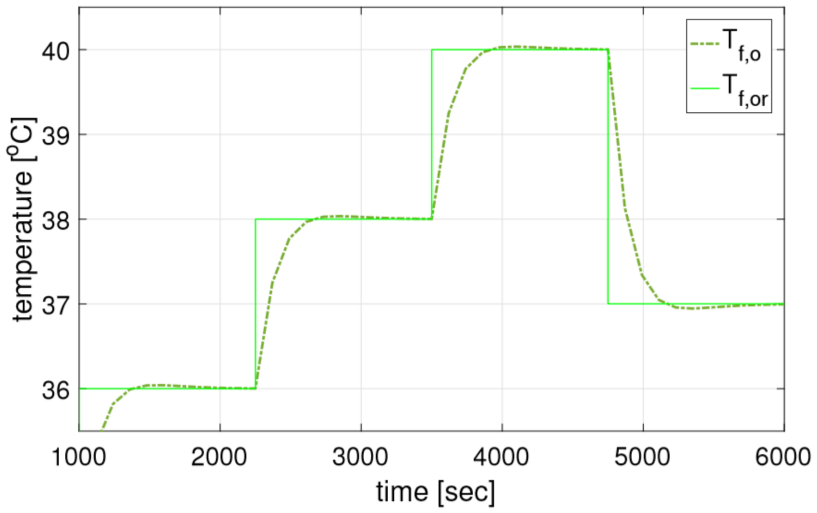

Response of PI-controller with constant solar radiation.

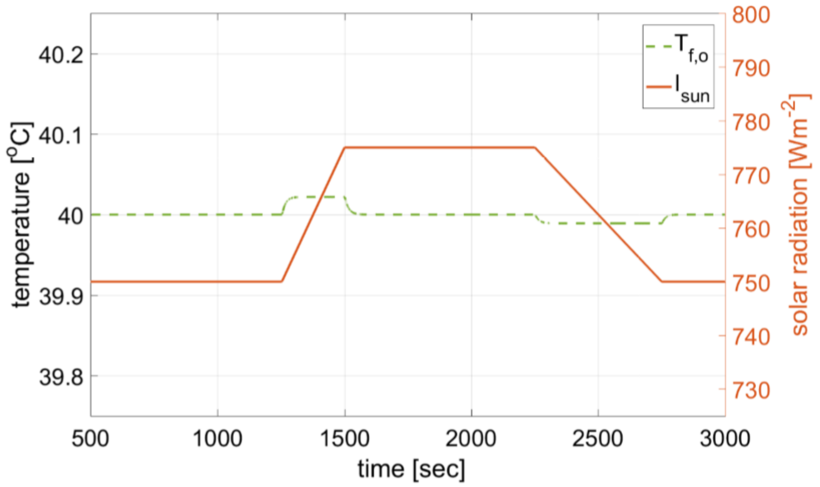

Tracking of desired temperature and disturbance rejection.

Control

H-infinity Feedback Control

- Designed for air-based model-I
- Complex model
- Linearization
  - *Computation of the system's Jacobian matrices*
  - *Current operating point*
- Requires the solution of an algebraic Riccati equation at each timestep of the control algorithm
- The initial nonlinear thermal model of the collector is described in the form

$$\dot{x} = f(x, u, v)$$

- State vector x contains

$$x = \begin{bmatrix} x_1 & x_2 & x_3 \end{bmatrix}^T = \begin{bmatrix} T_g & T_c & T_i \end{bmatrix}^T$$

- Feedback control loop
- Control scheme

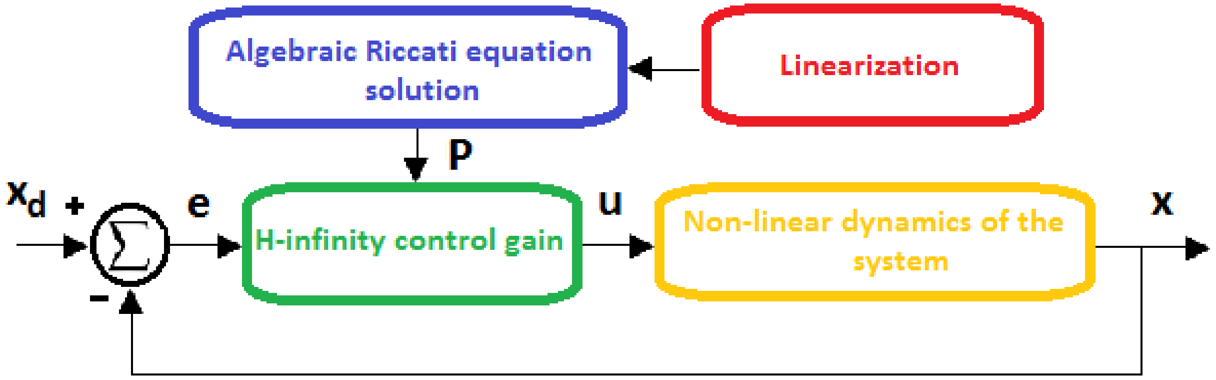

Control scheme for hybrid PV-T thermal model.

Control

Results

- Designed for air-based model-I
- Fast and accurate tracking of the reference setpoints
- External inputs directly affect the state temperatures
- Desired value of the states is updated
- Reference is tracked by rejecting effects of the disturbances.

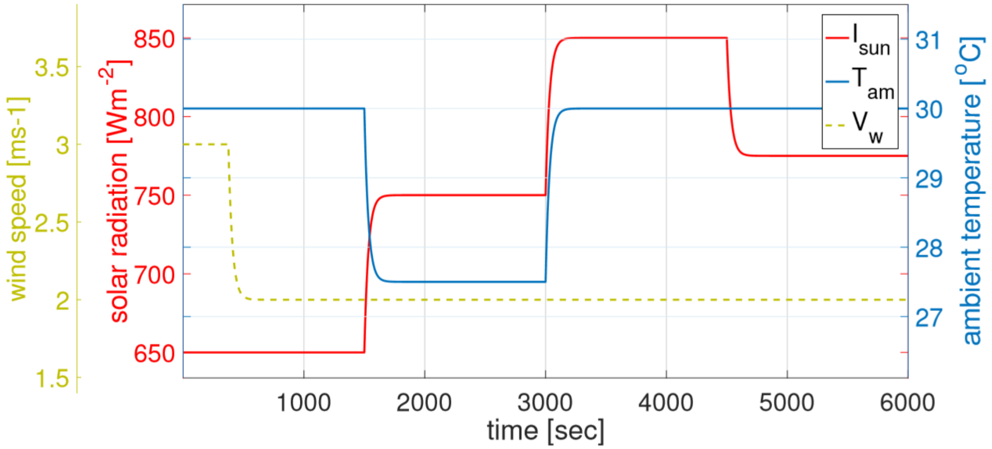

External inputs imposed on the system.

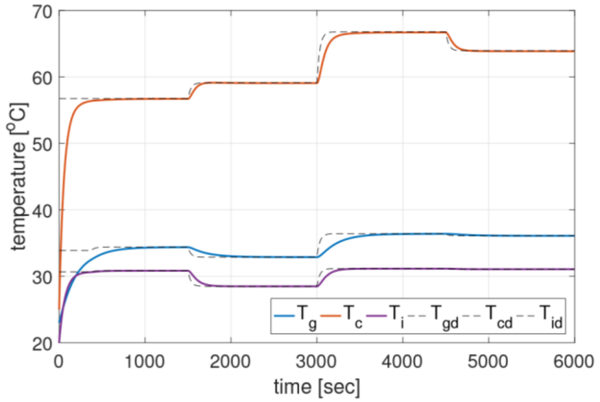

Tracking of reference setpoints by state variables.

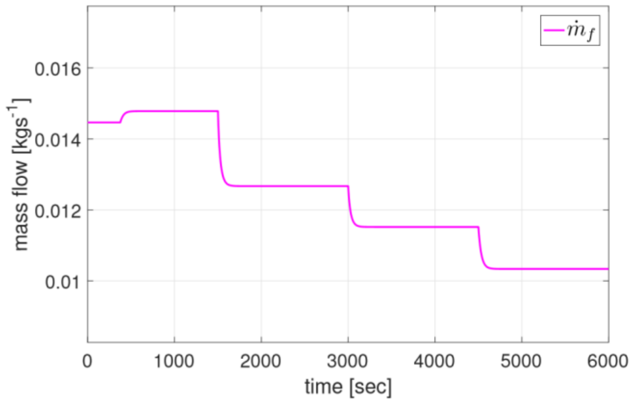

Evolution of the control input exerted.

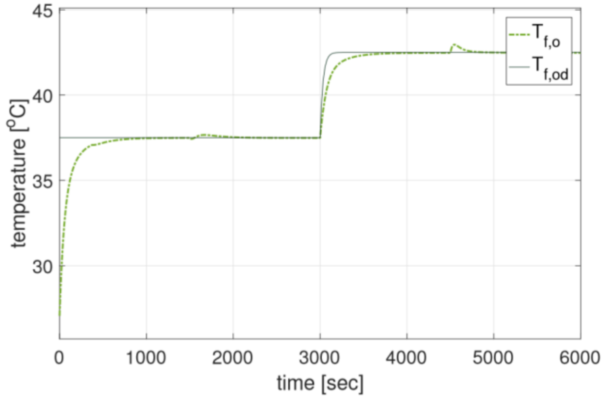

Evolution of the outlet temperature.

H-infinity Mixed Sensitivity Control

- General configuration with generalized plant
- Templates for the sensitivity functions S and KS
- Model is linearized around equilibrium points
- Transfer function is adequate for control
- Controller is calculated using function *hinfsyn*
- Order 5 to the order 2
- Model reduction approach using *balred*

$$K_{red}(s) = \frac{1.21e^{-7}s^2 + 0.12s + 1.80e^{-3}}{s^2 + 1.56e^{-2}s + 4.09e^{-5}}$$

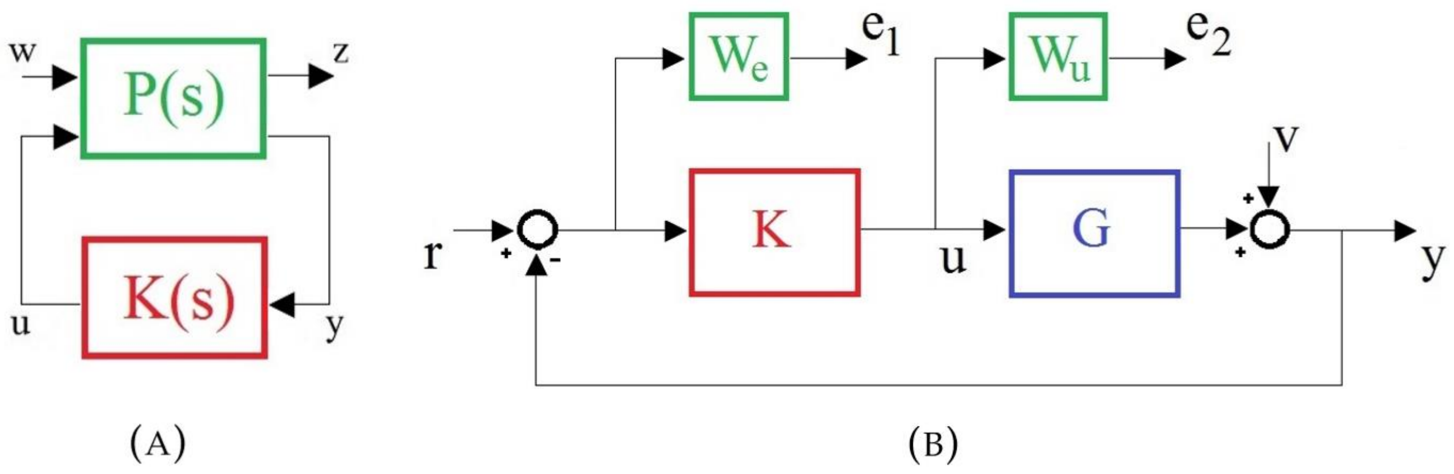

Fig. 72. (a) Generalized feedback system. (b) Complete control scheme.

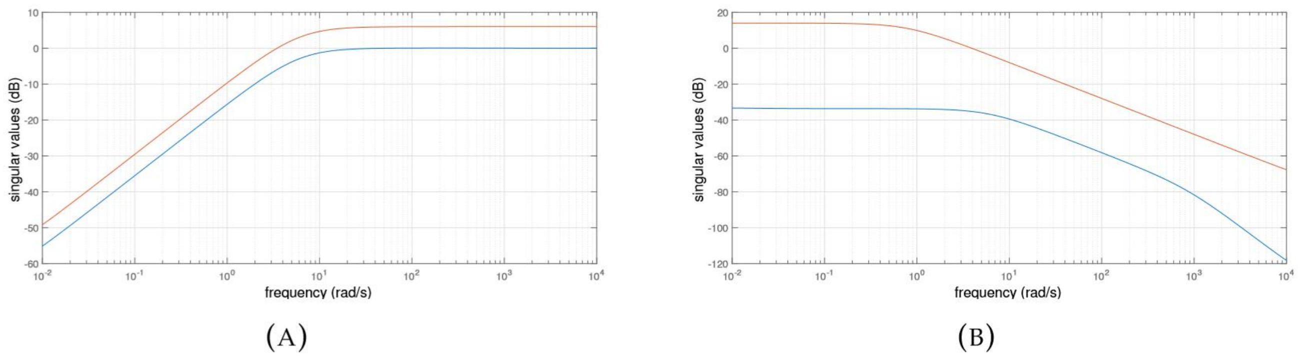

Fig. 73. Sensitivity functions of the robust control system: (a) Sensitivity function. (b) Controller*Sensitivity.

Control

Neural Network Control

- Levenberg Marquardt Backpropagatic algorithm is used
- Control input is injected to the real plant
- Reference is tracked even with external input
- Comparison of the controllers.

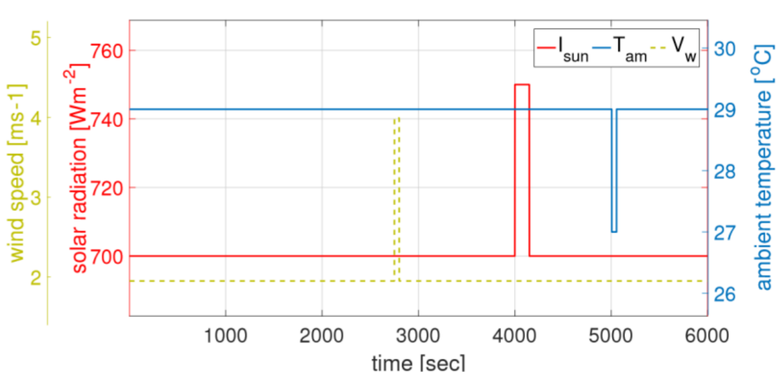

External inputs imposed on the system.

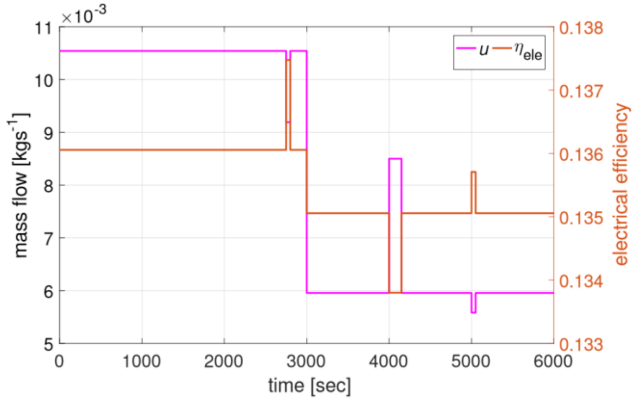

Evolution of the PV efficiency and control input.

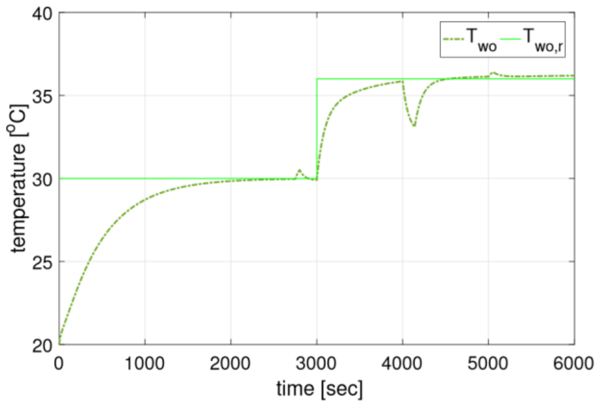

Evolution of the outlet temperature and disturbance rejection.

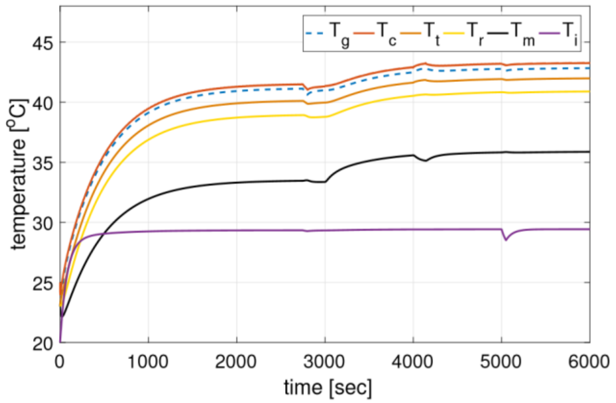

Evolution of state temperatures.

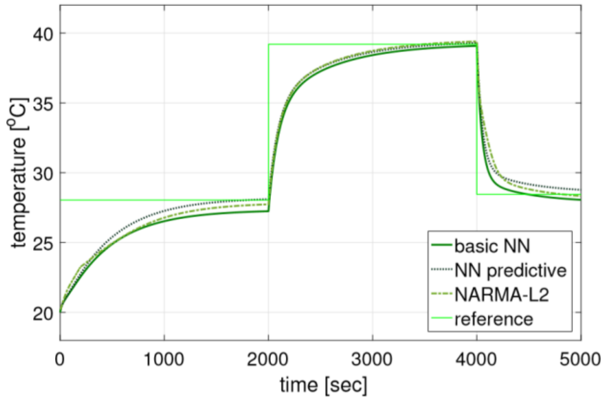

Response using basic controller, predictive controller and NARMA-L2 controller.

Control

Sliding Mode Control

- Designed for water-based model
- Advantage is that the closed-loop response becomes totally insensitive to some uncertainties once in the sliding mode
- Aim is to control the water output temperature
- *u* is the control input and *v* includes the external disturbances

- Sliding surface is described as;

$$S = y - y_{ref}$$

- If reachability condition $S\dot{S} < 0$ is fulfilled, the switching surface is known to be attractive
- The model was simulated using the following control law

$$u = u_c + u_{eq}$$

- u_c ensures convergence to chosen surface.

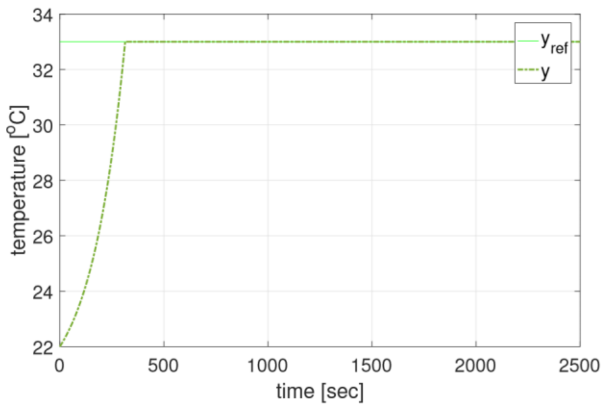

Convergence of output to the desired point.

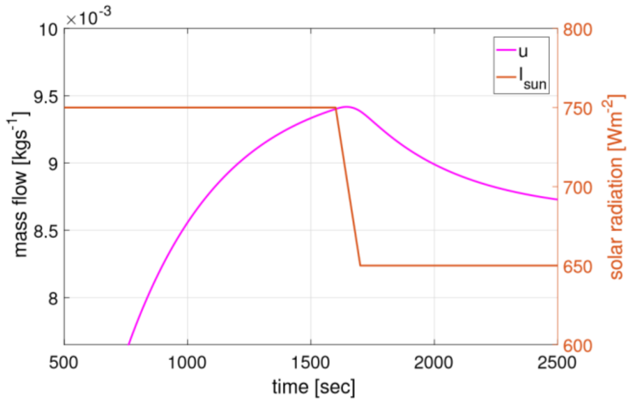

Control input with a change in solar radiation.

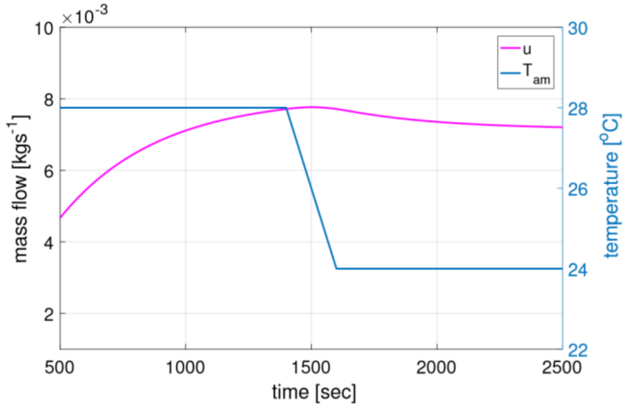

Control input with a change in ambient temperature.

Observer Design

- The objective is to design a nonlinear observer.

- Designing observers is a challenging problem due to its importance in automatic control design such as:
  - *control*
  - *monitoring*
  - *fault diagnosis.*

- $\overline{B}(\overline{x})$ can be written as:

$$\overline{B}(\overline{x}) = \frac{-f_2 C^T C}{4}\overline{x}$$

- The observer for the system is given by:

$$\begin{cases} \dot{\hat{\overline{x}}} = \sum_{i=1}^{2} \mu_i A_i \hat{\overline{x}} - \frac{f_2 C^T}{4}\hat{y}u + \frac{f_2 C^T \overline{D}}{4} v u + g(\tilde{y}) + \delta \\ \hat{y} = C\hat{\overline{x}} + \overline{D} v \end{cases}$$

- Linear matrix inequality (LMI) is used to compute the observer gain.

Observer Design

Proposition:

An observer of system (15) is given by

$$\begin{cases} \dot{\hat{\bar{x}}} = \sum_{i=1}^{2} \mu_i A_i \hat{\bar{x}} - \frac{f_2 C^T}{4} \hat{y} u + \frac{f_2 C^T \overline{D}}{4} v u + g(\tilde{y}) + \delta \\ \hat{y} = C\hat{\bar{x}} + \overline{D} v \end{cases}, \tag{19}$$

where g($\tilde{y}$) is chosen as:

$$g(\tilde{y}) = \frac{f_2 C^T}{4} \tilde{y} + L_i C \tilde{\bar{x}} \tag{20}$$

which can also be written as:

$$g(\tilde{y}) = (L_i + \frac{f_2 C^T}{4}) \tilde{y} \tag{21}$$

and $L_i = L = (1/2) X^{-1} C^T$, $i = 1, 2$; X is the positive definite symmetric matrix satisfying the LMI's.

$$\begin{cases} A_i^T X + X A_i - C^T C < -2\gamma X, \quad i = 1, 2 \\ X > 0 \end{cases}, \tag{22}$$

where $\gamma > | f | > 0$, $(-f)$ being the lowest the fastest pole of (15).

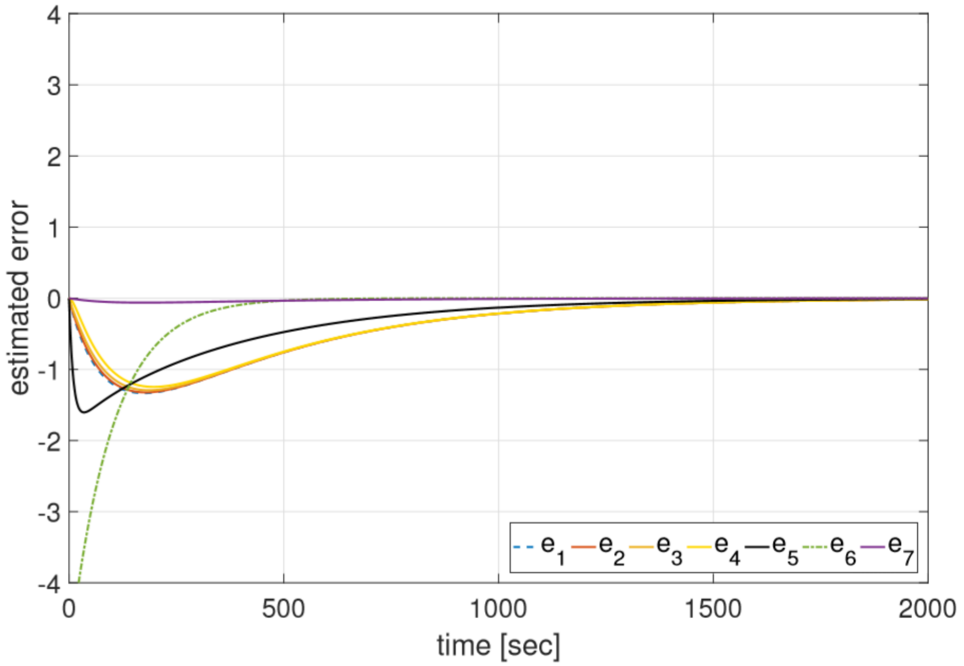

Estimation error.

Observer Design

Observer design with known inputs

- Designing observers is a challenging problem due to its importance in automatic control design such as:
  - *control*
  - *monitoring*
  - *fault diagnosis*
- Provide an estimate of the internal state of a plant
- Designed observer for water-based collector
- Multiple model developed is used

- The objective is to design a nonlinear observer
- $\overline{B}(\overline{x})$ can be written as:

$$\overline{B}(\overline{x}) = \frac{-f_2 C^T C}{4}\overline{x}$$

- The observer for the system is given by:

$$\begin{cases} \dot{\hat{\overline{x}}} = \sum_{i=1}^{2} \mu_i A_i \hat{\overline{x}} - \frac{f_2 C^T}{4}\hat{y}u + \frac{f_2 C^T \overline{D}}{4} v u + g(\tilde{y}) + \delta \\ \hat{y} = C\hat{\overline{x}} + \overline{D}v \end{cases}$$

- Linear matrix inequality (LMI) is used to compute the observer gain.

Observer Design

Observer design with unknown input (Water Inlet temperature)

- Objective is to construct an observer subjected to an unknown input
- Improvement in the design
- Multiple water-based model developed is used
- Lyapunov approach is used to ensure stability
- LMI is solved simultaneously
- Necessary and sufficient conditions for the existence of such approach are given

- Unknown input observer for the system is described as;

$$\begin{cases} \dot{z}(t) = \sum_{i=1}^{2} \mu_i D_i z(t) + Ez(t)u(t) + \sum_{i=1}^{2} \mu_i L_i Y(t) \\ \qquad +Jv(t) + Hu(t)Y(t) \\ \hat{\hat{x}}(t) = z(t) + MY(t) \end{cases}$$

- System is unknown input state observer if and only if

$$\lim_{t \to \infty} \| \hat{x}(t) - x(t) \| = 0$$

- Solar radiation and ambient temperature are not chosen as unknown inputs
- Fluid inlet temperature cannot be taken as unknown input because measured output contains it.

Observer Design

Results

- Initially simulated without any unknown input
- Choosing systems and observer initial conditions randomly
- A sinusoidal input is injected with similar conditions

- Real states are tracked by the observer states
- The results clearly agrees with the theory made on the observer exponential convergence
- A small effect on the states.

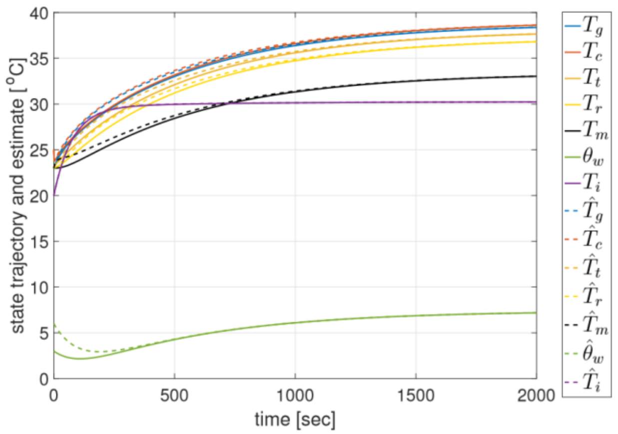

True states and their estimations without unknown input.

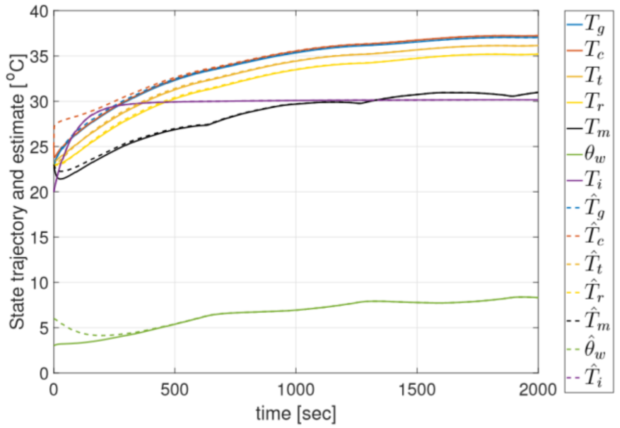

True states and their estimations with sinusoidal input T_{wi}.

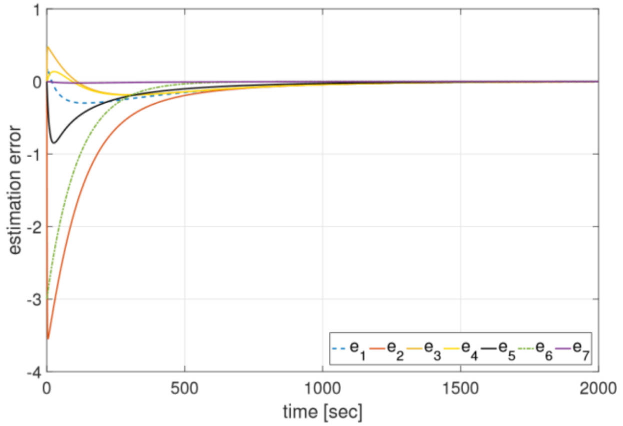

State estimation error.

Applications

The applications of the PV-T system are classified according to their temperatures.

- *Low-temperature applications take in heat pump systems and heating swimming pools or SPAs up to 50ºC.*
- *Medium-temperature applications are found in buildings for domestic hot water and space heating where the temperature of up to 80ºC is required.*
- *High-temperature applications with a temperature above 80ºC are required for certain industrial processes, e.g., desalination and agro-industrial processes.*

The applications include:

Building

- Most common application
- Mounted on the walls
- Occupies less space
- Better efficiency
- Energy obtained can be utilized for domestic water heating and space heating.

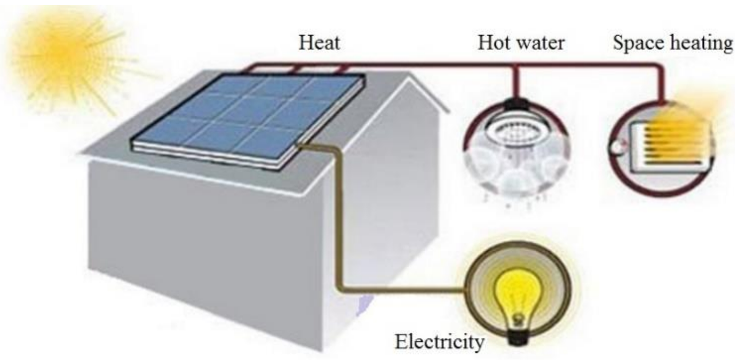

PV-T roof-top array supplying heating and electricity to building

Greenhouse drying

- Popular in developing countries
- Preservation of agricultural products and food
- Dried products are very good source of nutrients
- High temperature may damage the product and the germination capacity.

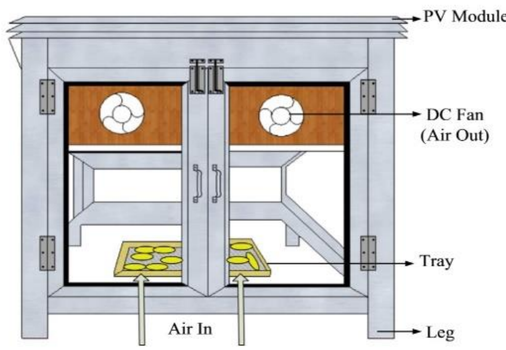

Greenhouse dryer

Applications

Desalination

- Promising solution to obtain drinking water
- Can be used for irrigation purpose
- Requires high temperature
- Useful in remote areas and isolated islands.

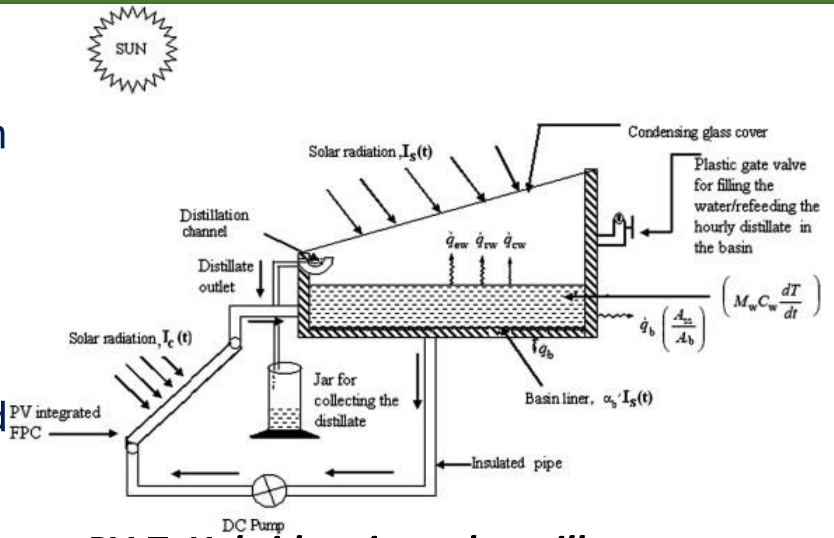

PV-T Hybrid active solar still

District heating/cooling

- Requires large space/area
- Parabolic trough collectors are recommended
- Useful for regions such as the Mediterranean, Gulf, and South Asia.
- Benefits include community energy management, safer operation, increased reliability, and reduced operation costs.

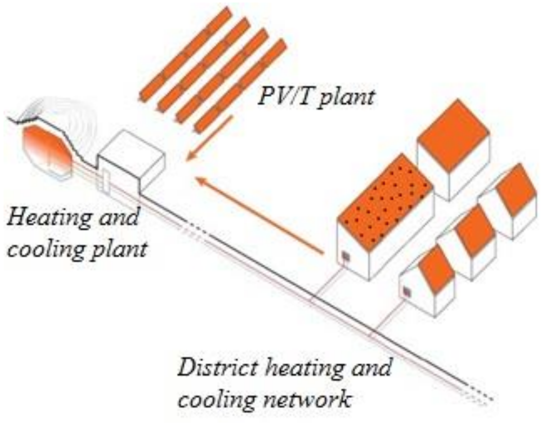

Fig. 10: PV-T district heating and cooling.

Refrigeration

- It can be used in medical laboratories, marts, and slaughter houses
- Especially for isolated islands and coastal regions.

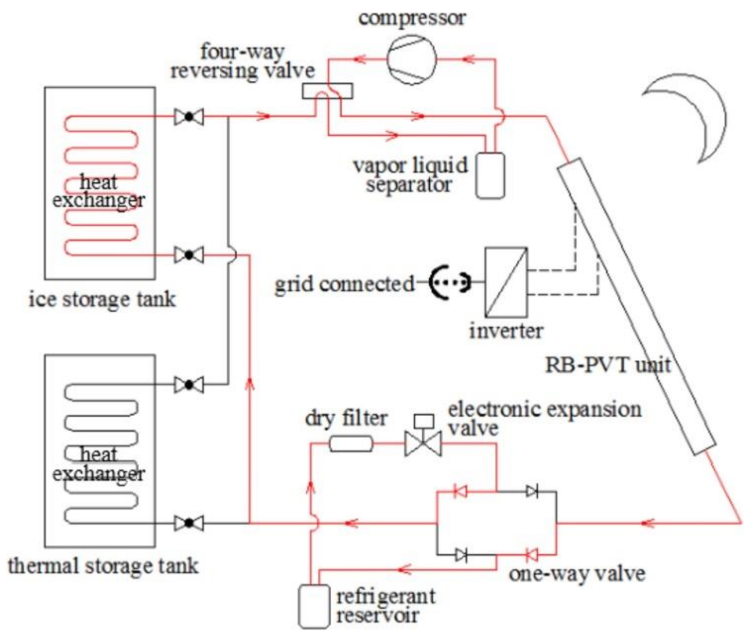

Schematic diagram of the proposed PV-T heat pump system on refrigeration mode

Drying

- Drying is a fundamental process in many industrial applications.
- Popular in developing countries for the preservation of agricultural products.
- Dried products are a very good source of nutrients.
- It is very critical process and must ensure that the dried material satisfies recomm specifications.
- Control is important in order to guarantee the quality of dried products in terms of
  - *Color*
  - *Visual aspect*
  - *Flavor*
  - *Retention of nutrients*
  - contaminants content.
- A lot of research has been done and is always ongoing.

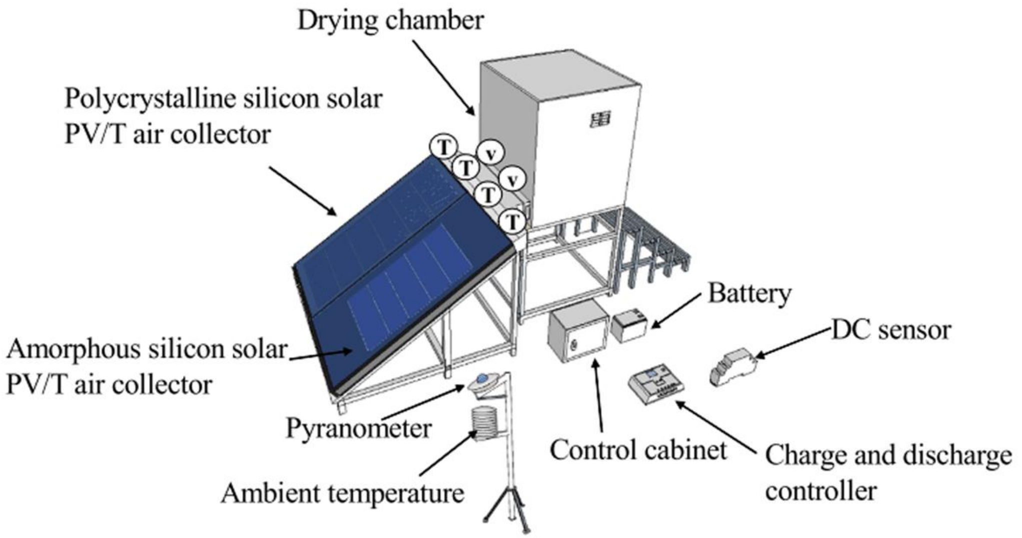

Schematic diagram of PV/T drying system.

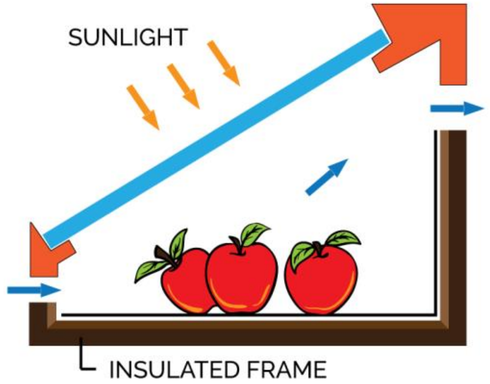

Solar dryer.

CENTER FOR ADVANCED RESEARCH IN DRYING

Applications

- Useful thermal output used for drying.
- Waste heat at the outlet air can also be recovered.
- Input temperature is proportional to the output air under recycling scenario.
- Electricity generated by the PV/T can be stored and used when needed.
- Output air temperature can be close to its maximum if:
    - ✓ *The recycling efficiency is high*
    - ✓ *The air flow rate is low.*
- Only needed to set the air flow rate to a low value that allows:
    - ✓ *The collection of the heat from solar energy*
    - ✓ *The moisture removal*
    - ✓ *The heat recovery from the outlet air.*

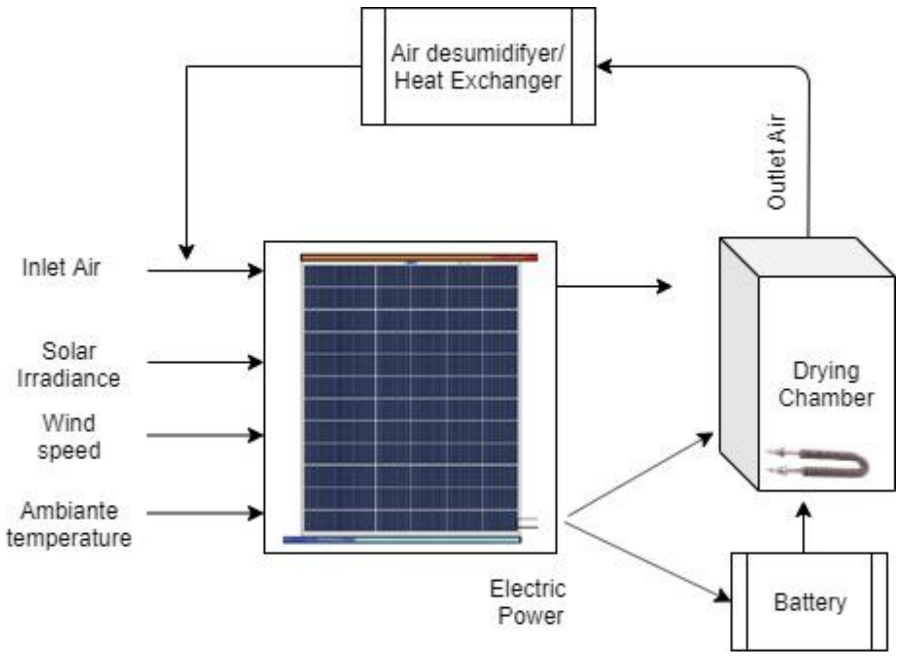

Solar dryer with air recirculation.

Solar Living Lab

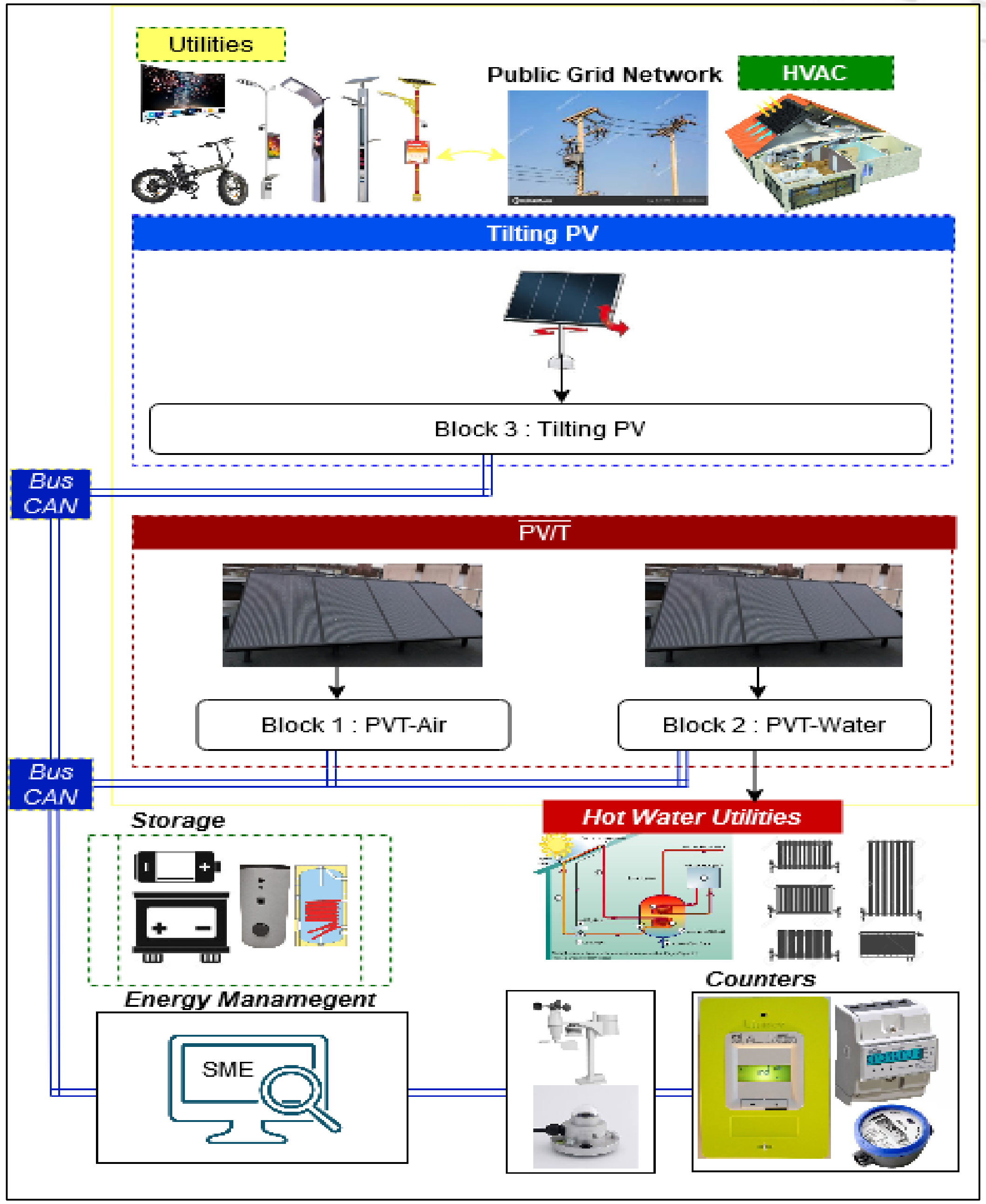

Thermal part

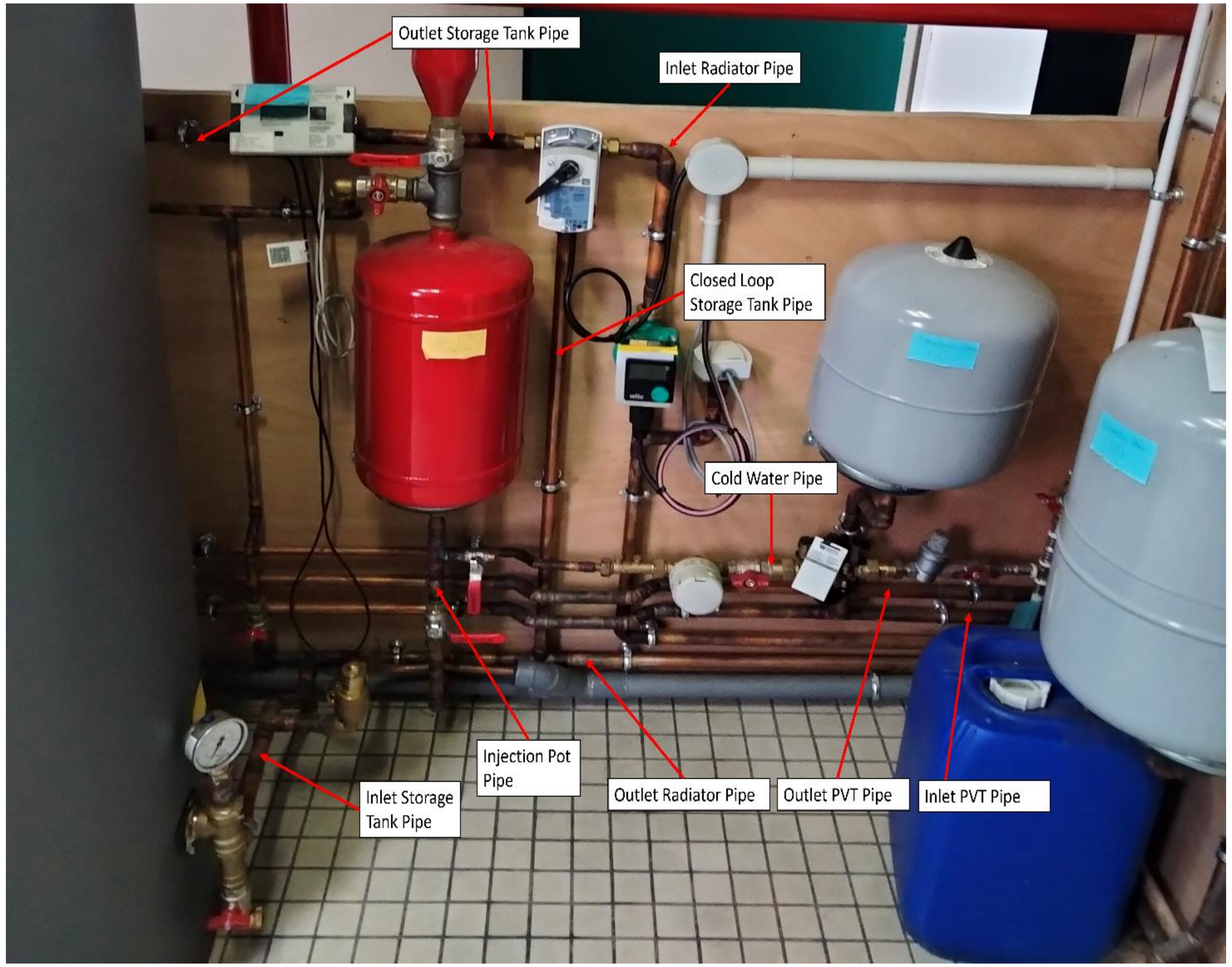

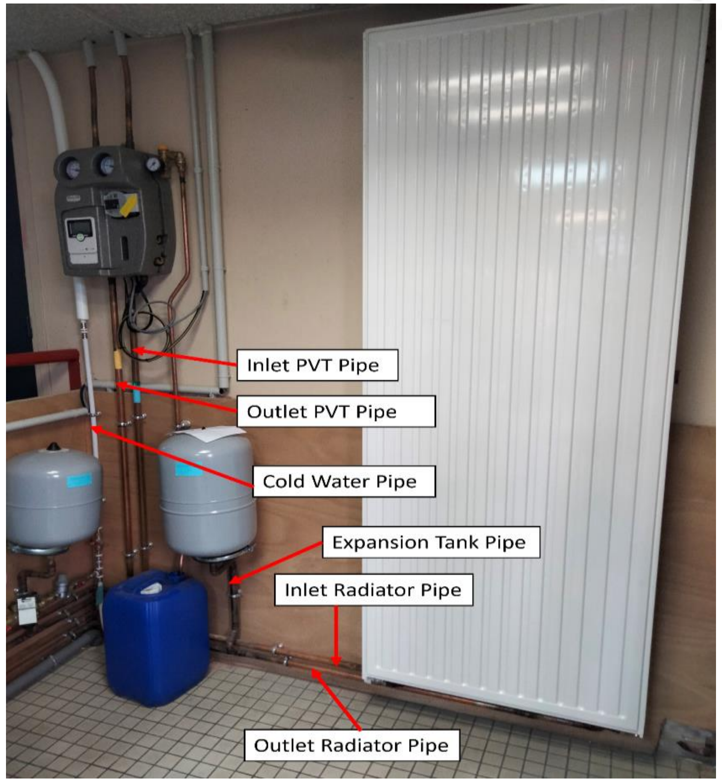

EE Architecture - SOLLAB

Process Monitoring of *SOLLAB*
CAN Bus Option

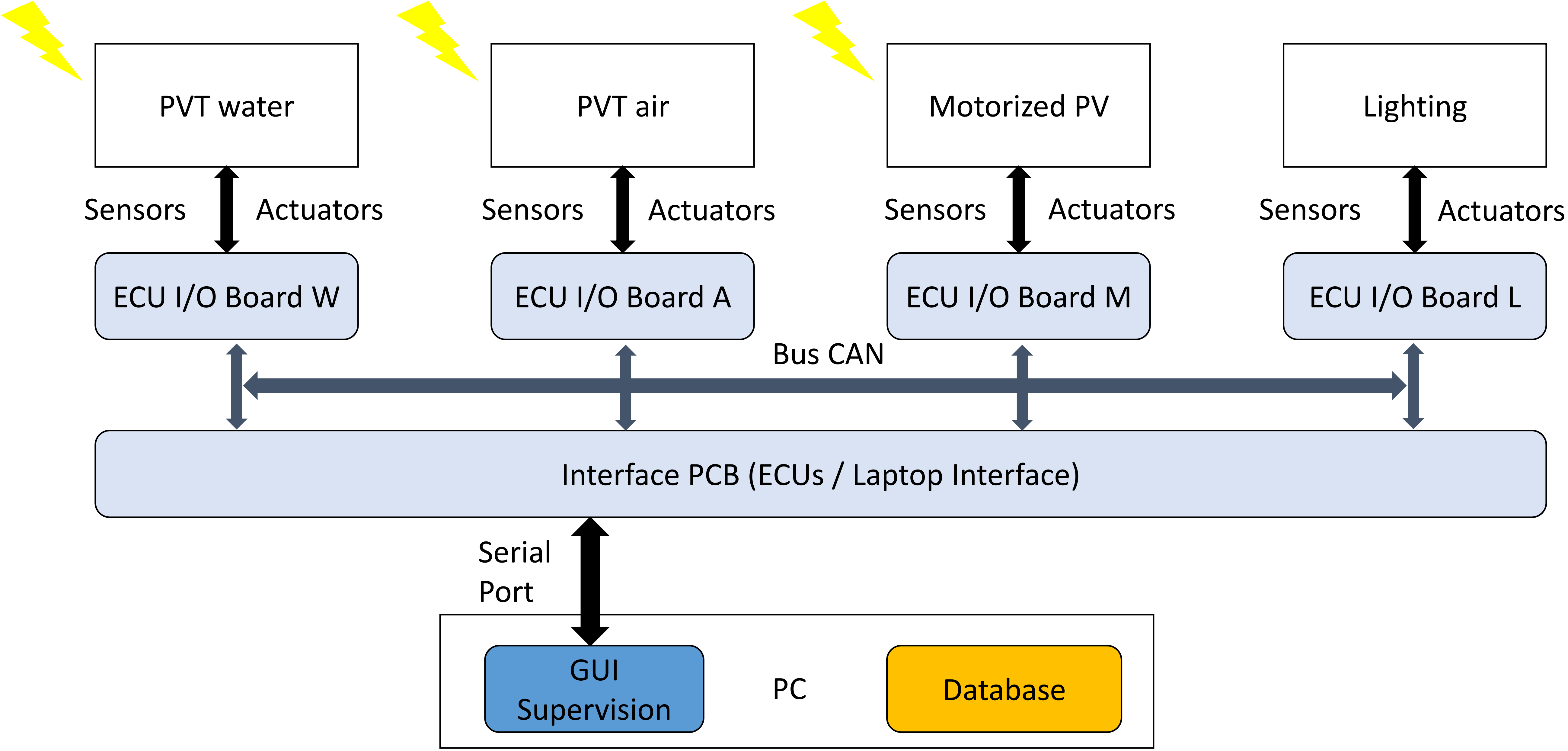

EE Architecture - SOLLAB

Process Monitoring of *SOLLAB*
Wireless Option

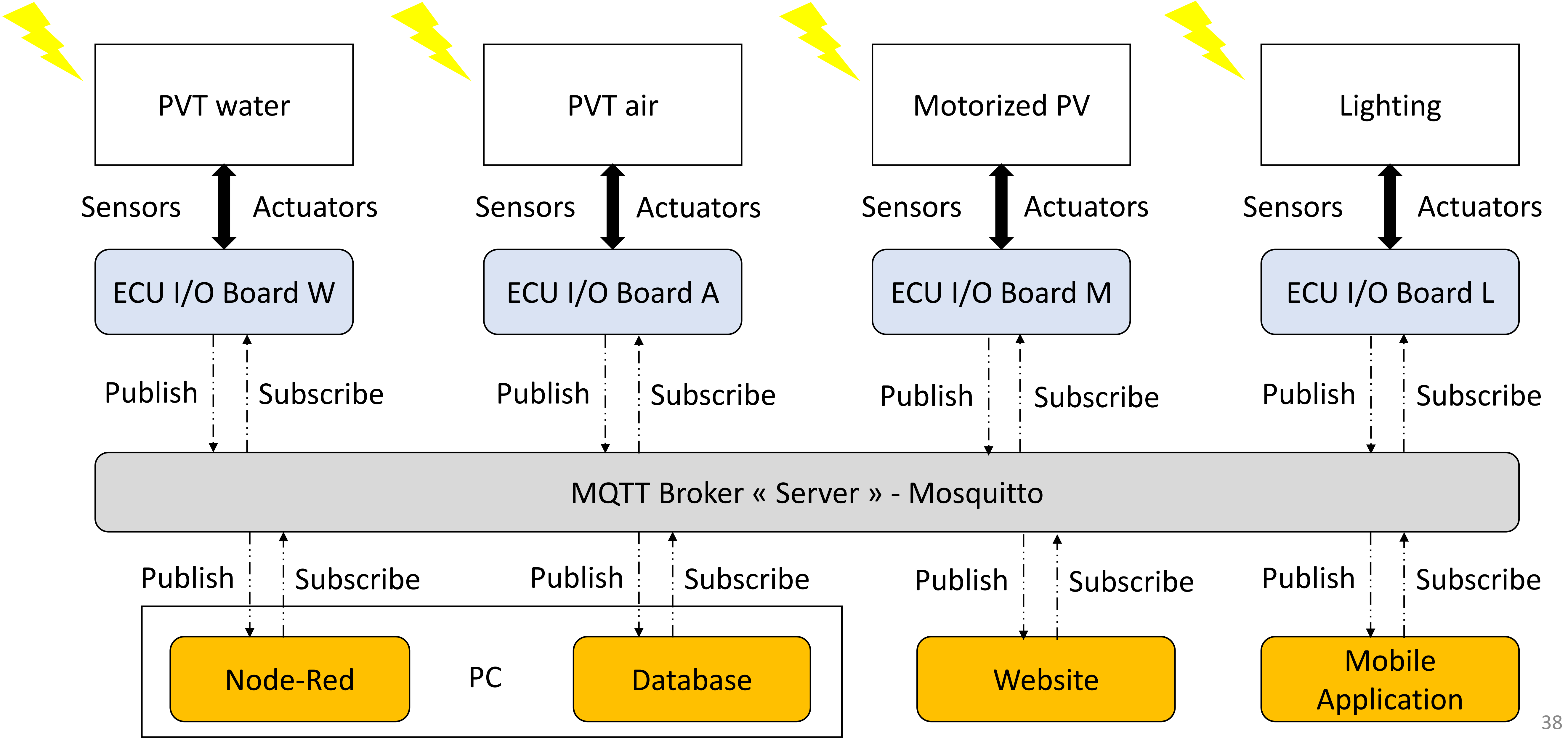

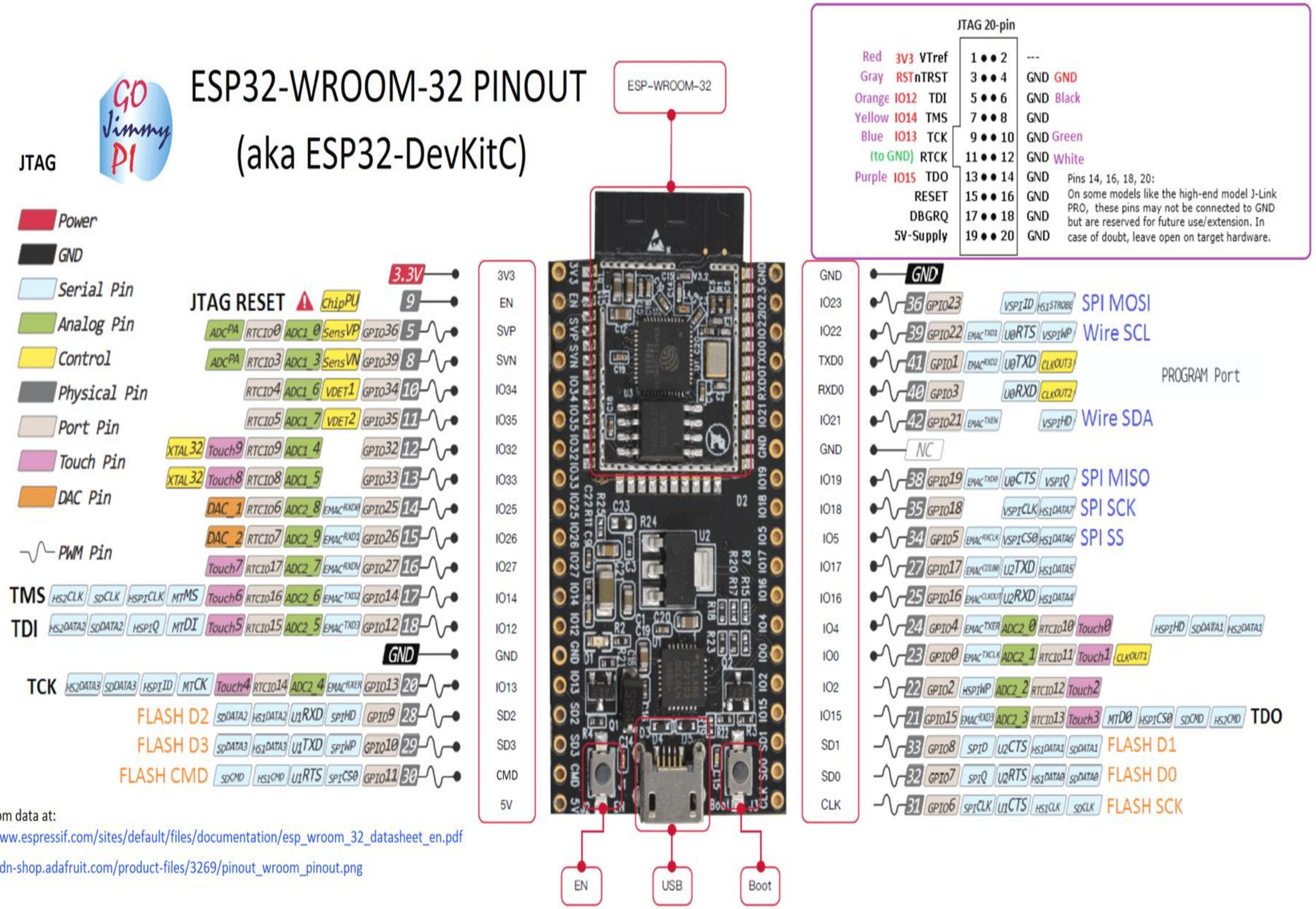

Adapted from data at:

http://www.espressif.com/sites/default/files/documentation/esp_wroom_32_datasheet_en.pdf

https://cdn-shop.adafruit.com/product-files/3269/pinout_wroom_pinout.png

1	3V3	3V3	x		20	x	GND	GND	
2	EN		x		21	MicroSD	VSPI MOSI	IO23	GPIO23
3	SVP	A36	Input A	GPIO36	22	RTC	I2C-SDL	IO22	GPIO22
4	SVN	A39	Input A	GPIO39	23	Program Debug/Nextion	TXD0	TXD0	GPIO1
5	IO34	A34	Input A	GPIO34	24	Program Debug/Nextion	RXD0	RXD0	GPIO3
6	IO35	A35	Input A	GPIO35	25	RTC	I2C-SDA	IO21	GPIO21
7	IO32	A32	Input A	GPIO32	26	x	GND	GND	
8	IO33	A33	Input A	GPIO33	27	MicroSD	VSPI MISO	IO19	GPIO19
39	IO25	DAC_1	Output A	GPIO25	28	MicroSD	VSPI SCK	IO18	GPIO18
10	IO26	DAC_2	Output A	GPIO26	29	Bus CAN	CAN Tx	IO5	GPIO5
11	IO27	LED_27	Output-D	GPIO27	20	SIM800L-RX	TXD2	IO17	GPIO17
12	IO14	RXD1	GPS-TX	GPIO14	31	SIM800L-TX	RXD2	IO16	GPIO16
13	IO12	TXD1	GPS-RX	GPIO12	32	Bus CAN	CAN Rx	IO4	GPIO4
14	GND	GND	x		33	DRIVE/STOP	MOS_PIN	IO0	GPIO0
15	IO13	Temp	Input D	GPIO13	34	Buzzer 3.3V	BUZZ_PIN	IO2	GPIO2
16	SD2			GPIO9	35	MicroSD	CS	IO15	GPIO15
17	SD3			GPIO10	36			SD1	GPIO8
18	CMD			GPIO11	37			SD0	GPIO7
19	5V	5V	x		38			CLK	GPIO6

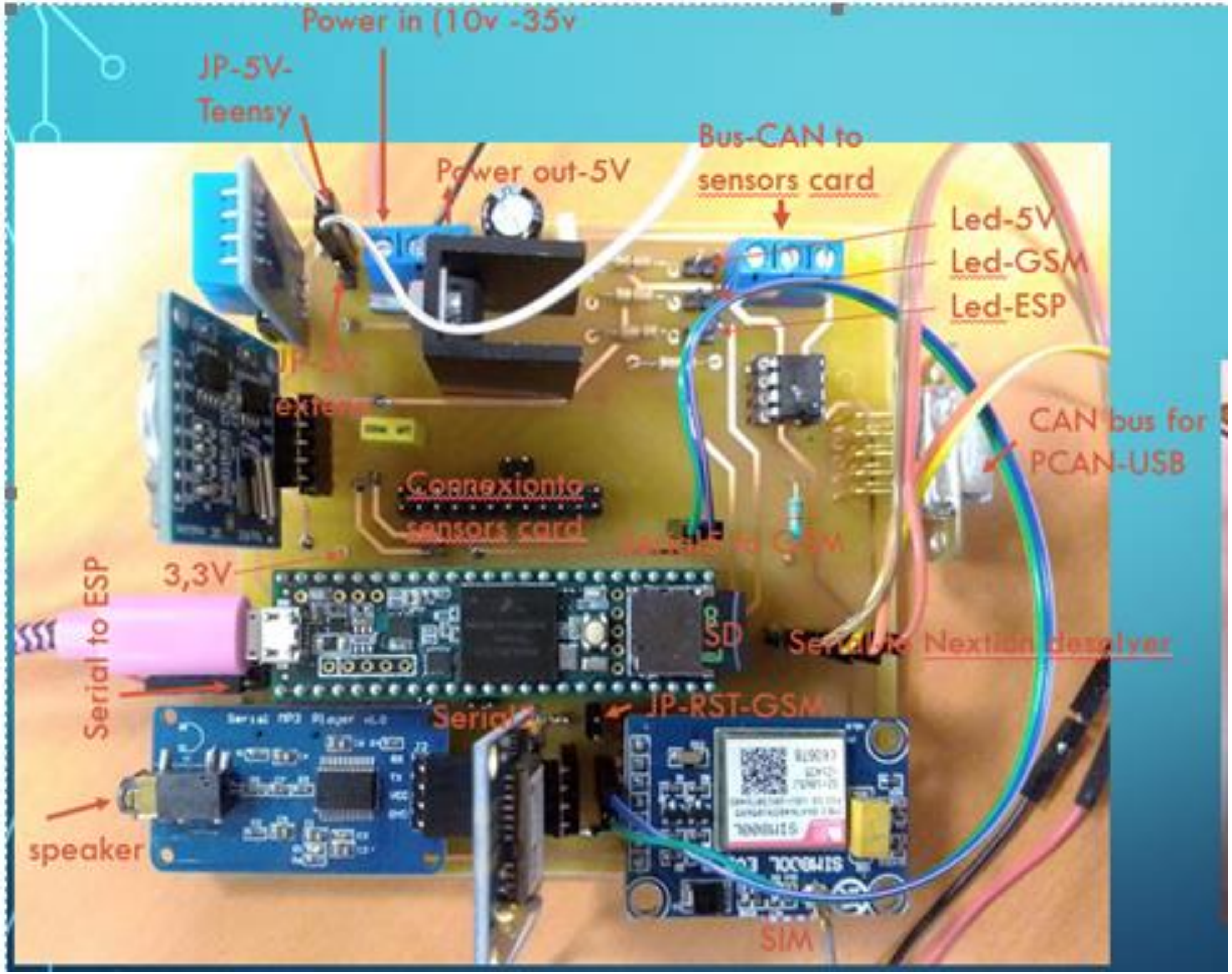
Power in (10v -35v
JP-5V-
Teensy
Power out-5V
Bus-CAN to
sensors card
Led-5V
Led-GSM
Led-ESP
CAN bus for
PCAN-USB
Connexionto
sensors card
3,3V
Serial to ESP
SD
Nextion
JP-RST-GSM
speaker
SIM


19°C
43 %
M/A
Frein
08:49
24/1/2020
C.I.
Niv.B.
0000 Km
00 Km
-24A
12 %
Max
45
49.89815
2.29673
4
Km/h
00 Km
D
A

ioT Datalogger

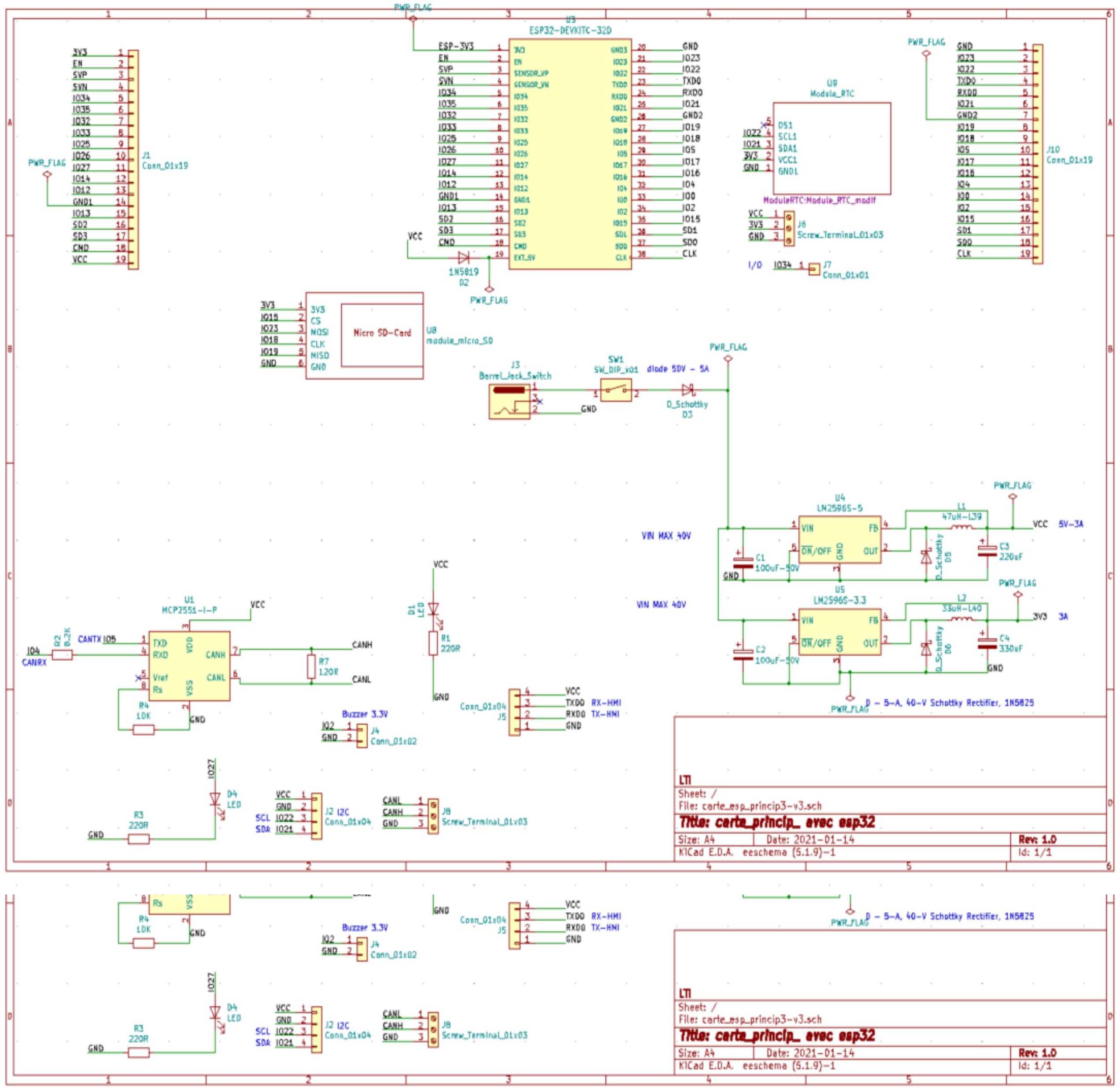

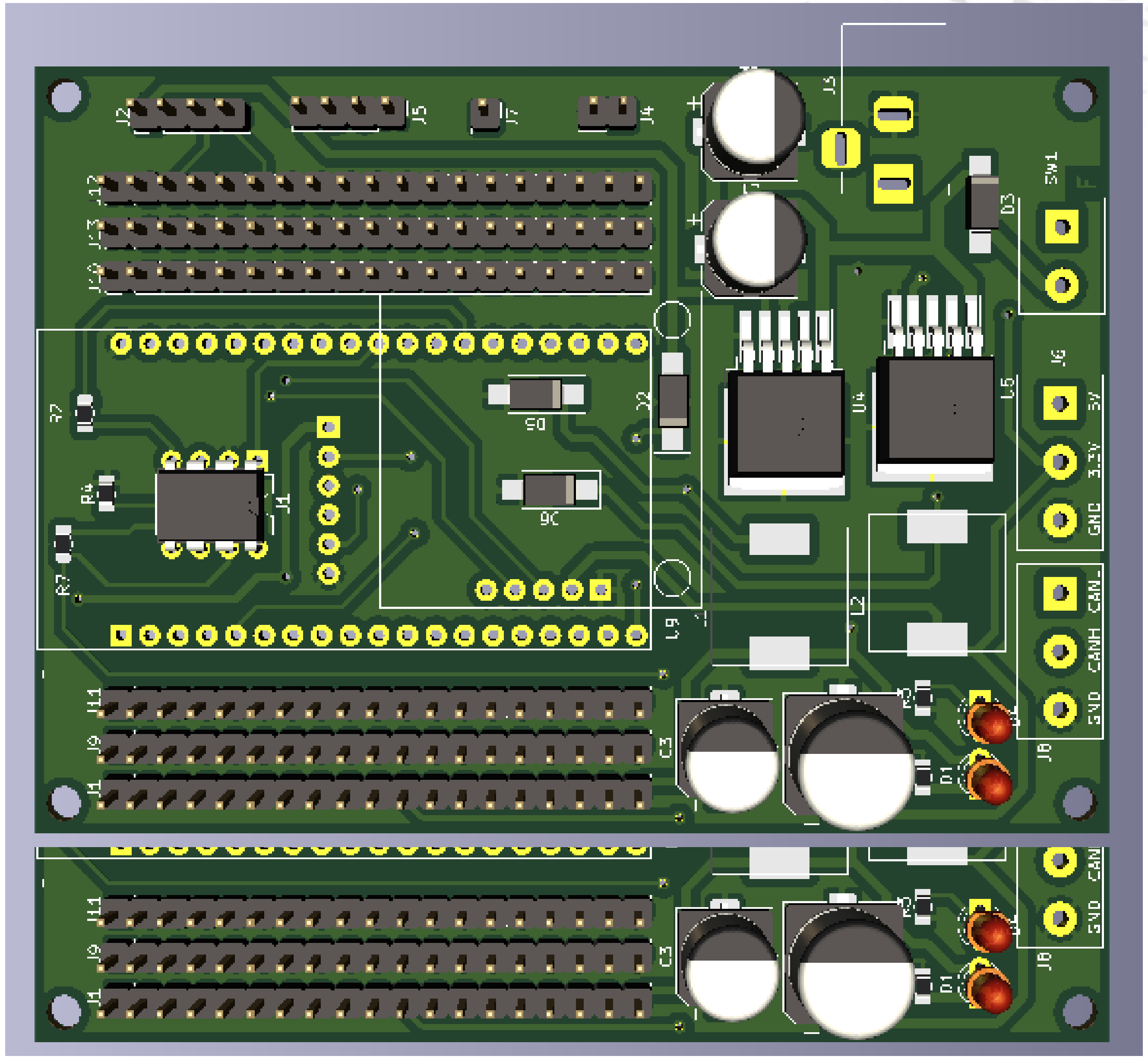

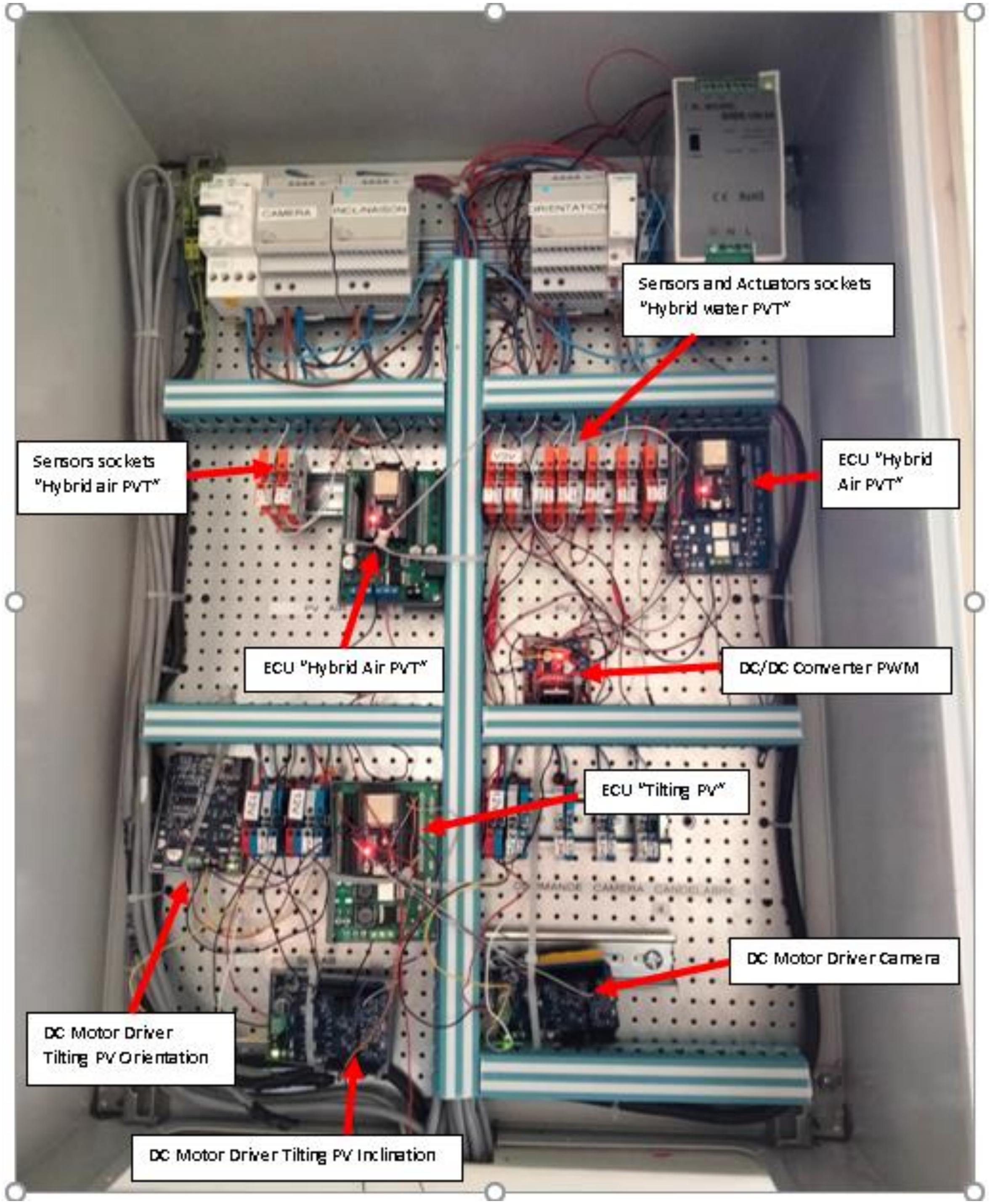
Sensors and Actuators sockets "Hybrid water PVT"
Sensors sockets "Hybrid air PVT"
ECU "Hybrid Air PVT"
ECU "Hybrid Air PVT"
DC/DC Converter PWM
ECU "Tilting PV"
DC Motor Driver Camera
DC Motor Driver Tilting PV Orientation
DC Motor Driver Tilting PV Inclination

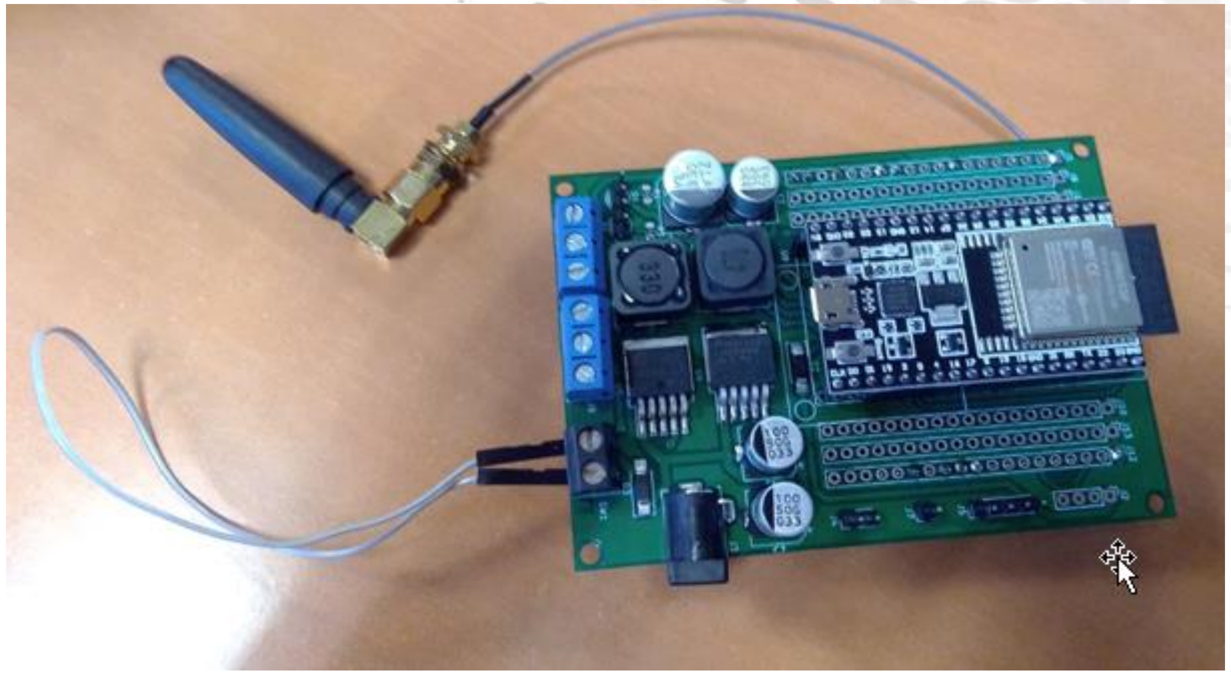


ESP-NOW
Two-way communication

Node-Red - MQTT

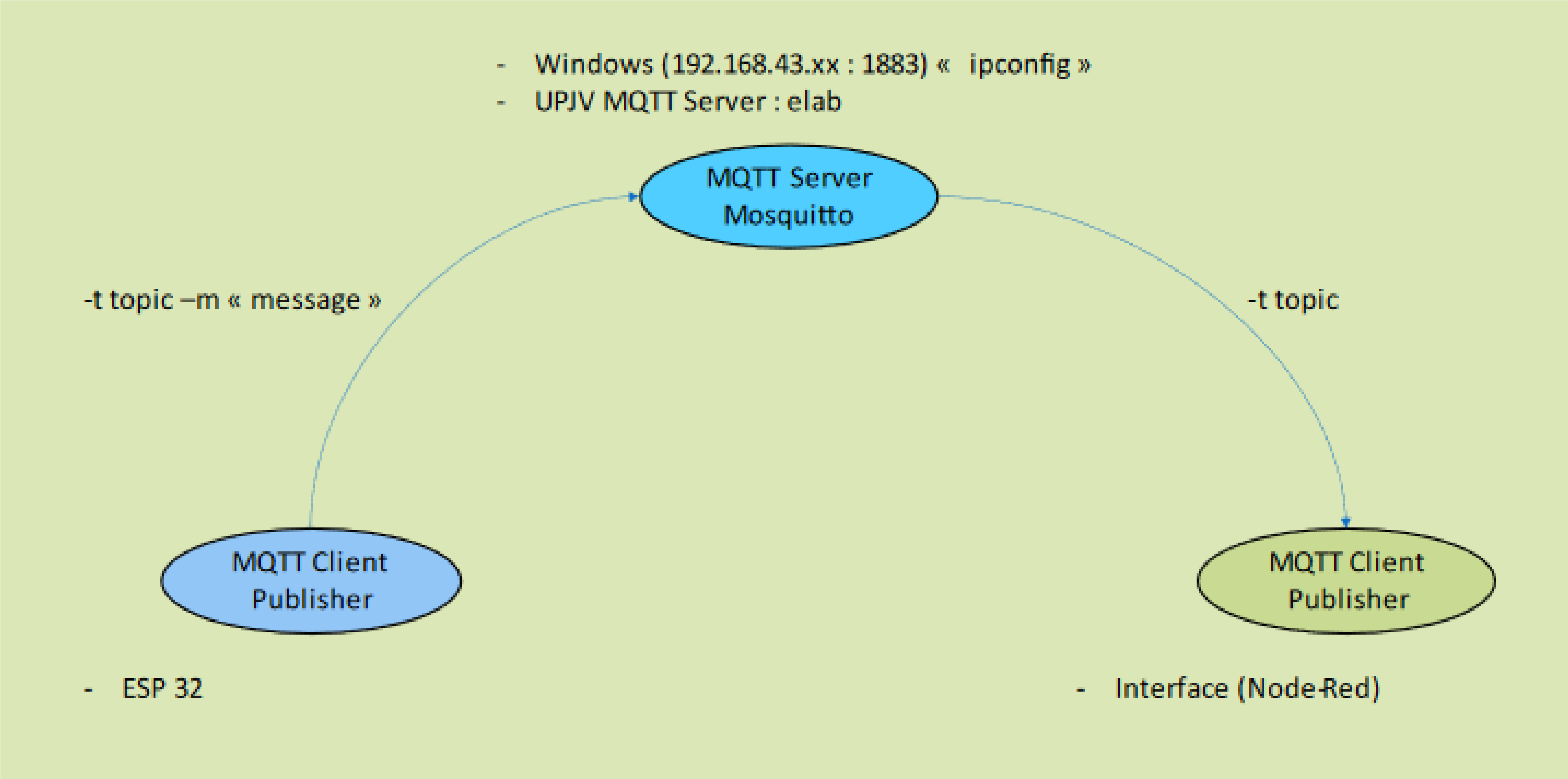

https://elab.u-picardie.fr/ui/

Thank you for your attention

This work was carried out as part of the SOLARISE project of the Interreg 2 Seas 2014-2020533 programme co-financed by the European Regional Development Fund sub-grant contract No. 2S04-004.